Grafted mesoporous silicas for radionuclide uptake: Radiolytic stability under electron irradiation

Guillaume Zante, Vincent Bouniol, Saad Sene, Cyrielle Rey, Jérémy Causse, Joulia Larionova, Yannick Guari, Xavier Deschanels, Sophie Le Caër

Grafted mesoporous silicas for radionuclide uptake: radiolytic stability under electron irradiation

Guillaume Zante,[a] Vincent Bouniol,[b] Saad Sene,[b] Cyrielle Rey,[c] Jérémy Causse,[c] Joulia Larionova,[b] Yannick Guari,[b] Xavier Deschanels[c] and Sophie Le Caër[a*]

[a] *Université Paris-Saclay, CEA, CNRS, NIMBE, UMR 3685, 91191, Gif-sur-Yvette, France*

[b] *ICGM, Université de Montpellier, CNRS, ENSCM, Montpellier, France*

[c] *ICSM, Université de Montpellier, CEA, CNRS, ENSCM, Bagnols-sur-Cèze 30200, France*

*Corresponding author

E-mail address: sophie.le-caer@cea.fr; phone: +33 1 69 08 15 58; fax: +33 1 69 08 34 66

Highlights

● SBA-15 silica was grafted with hydroxypiridinone and phosphonate ligands

● Under irradiation, amide functional groups were the most sensitive to damage

● Reaction mechanisms under irradiation are discussed

● These mechanisms strongly depend whether the ligand molecule is grafted on mesoporous silica or not

● In SBA-15 grafted with propionamide phosphate, Th(IV) sorption is not significantly changed by irradiation up to a few MGy

Abstract

Materials developed for radionuclide adsorption need to resist harsh conditions, i.e. be robust against ionizing radiation. In this work, we evaluated the degradation of mesoporous silicas (SBA-15) grafted with hydroxypiridinone, acetamide phosphonate and propionamide phosphonate ligands under electron irradiation. The ligands contained amide and phosphinic acid functional groups, which made them able to bind to actinides. Degradation of the grafted ligand was assessed by identifying and quantifying the gas produced under irradiation using gas

chromatography, as well as characterizing the grafted ligands before and after irradiation by means of FT-IR, XPS and TGA techniques. Irradiation led to the degradation of amide functional groups and to the production of amine and carboxylic acid groups. Corresponding reaction mechanisms were proposed. The sorption behavior of the grafted SBA-15 materials for thorium was also studied. SBA-15 materials grafted with acetamide phosphonate and propionamide phosphonate ligands were shown to be able to adsorb thorium. The propionamide phosphate ligand was the most efficient, with an equilibrium sorption capacity of 95 $mg \cdot g^{-1}$. This capacity remained stable up to a 1 MGy irradiation dose and underwent a 20% decrease after 4 MGy of irradiation. Therefore, this material is potentially interesting for the treatment of liquid outflows contaminated by actinides produced in nuclear facilities.

Keywords: electron irradiation; grafted mesoporous silica; functionalized SBA-15; reaction mechanisms; actinide adsorption; nuclear waste management

1. Introduction

The nuclear industry generates radioactive wastes containing various elements. Among them, the most concerning are actinides such as plutonium and minor actinides (neptunium, americium and curium) due to their radiotoxicity and long half-lives [1]. These elements can be found at very low concentration in contaminated aqueous wastes [2], and in organic wastes from nuclear fuel reprocessing facilities [3]. In both cases, the standard approach for handling these wastes is geological disposal [4], which necessitates first the recovery of the radioactive materials from the liquid stream before their immobilization within solid matrices (e.g. glasses and cements).

Therefore, there is a need for efficient methods to capture actinides from liquid wastes. Adsorbents such as mesoporous silica have attracted attention due to their interesting properties such as a high specific surface area, tunable pore sizing and high adsorption capacity [5]. Moreover, these materials can be functionalized easily using soft chemistry methods, such as sol-gel synthesis, in order to graft specific ligands. This allows not only the enhancement of the adsorption capacity of the material, but also the targeting of specific elements ([6-10]).

Functionalized silicas have been used for the extraction of lanthanide [11-12] and actinide ions [13-16] as well as for heavy metals [17]. Indeed, some functionalized silica materials display

higher adsorption capacity and faster adsorption kinetics than those of conventional ion exchange resins [7], confirming their potential. Moreover, the porosity of silica could be closed after (self-)irradiation, which would then combine both the benefits of sorption and storage of radionuclides [18-19].

Of course, the nature of the ligands incorporated in porous structures affects their sorption ability. Proper selection of the ligand is thus mandatory before grafting. For instance, carbamoylphosphonate ligands have a particular affinity for actinide ions [20], which makes their grafting promising for their selective capture. Hydroxypiridinone ligands have also been investigated for the bioremediation of actinides such as uranium [21]. The incorporation of this kind of ligand within the pores of mesoporous silica would lead to an efficient sorption of radionuclides [2].

However, despite these merits, the mesoporous sorbents must be robust towards harsh conditions, such as ionizing radiation at a high dose and/or at a high dose rate, when used for the capture of radionuclides [5]. For instance, ion exchange resins, commonly used to purify water contaminated by radioactive elements, must be able to resist a maximal dose rate of 100 $Gy \cdot h^{-1}$ (1 Gy = 1 $J \cdot kg^{-1}$) [22]. Gray (Gy) is the dose unit commonly used in radiation chemistry. It corresponds to the energy deposited in the matter per kilogram of matter. In this case, activated corrosion products such as ^{60}Co, a gamma radiation emitter, are responsible for the observed dose rate.

Damage caused by irradiation makes the renewal of the adsorbent necessary. For commonly used adsorbents such as ion exchange resins, irradiation damage depends on the type of materials and the dose adsorbed. Irradiation damage was found to start at doses ranging between 1 kGy and 10 MGy under gamma irradiation, depending on the nature of the resin [23-24]. Therefore, the behavior of these materials towards irradiation requires investigation and understanding of the reaction mechanisms at play. This knowledge will enable the proper selection of ligands able to resist a high dose of irradiation, a crucial parameter concerning actinide extraction. For example, materials that incorporate 10 wt% of Pu within their structure receive a dose of 10^7 Gy after one year of storage [25-26]. The potential sorbent material must therefore fulfill two important requirements: the ability to (i) retain radionuclides and (ii) to continue functioning properly in a highly radioactive environment.

To date, irradiation of mesoporous SBA-15 silica grafted with various ligands has been studied using gamma irradiation [23, 27-28]. However, the dose accumulated in these studies was quite low (from 10 kGy to 500 kGy). Zhang *et al.* [28] showed that phosphine oxide and phosphinic acid ligands grafted on a SBA-15 matrix retain their sorption ability when irradiated up to 500 kGy. Iqbal *et al.* [23, 27] evidenced no or little reduction of the sorption ability of ethylenediaminetetraacetic acid, aminopropyl and N-propylsalicyl-aldimino grafted SBA-15 irradiated up to 1 kGy. In the case of grafted controlled pore glasses, electron irradiation was performed up to a dose of 500 kGy [29-30] and significant modifications of the materials could be evidenced, depending on the nature of the grafted molecules. In these studies, ionizing radiation creates electron-hole pairs within the material that can recombine to form excitons if the walls of the materials are thick enough [31]. These species can then be transferred to the interface where they damage the grafted ligands.

In the present study, our aim was to explore the effect of electron irradiation, used to mimic the irradiation effects of sorbed radionuclides, on grafted mesoporous silica and to assess its stability up to a few MGy, a dose higher than that used in the articles cited above. We decided to work with SBA-15 silica (Santa Barbara Amorphous n°15, [32]) rather than with MCM-41 (Mobil Crystalline Materials n°41, [33]), since SBA-15 was shown to be more robust towards ionizing radiation than MCM-41, probably due to its larger pore size [18]. Three ligands were selected and grafted on SBA-15 materials. The choice of ligands was motivated by their ability to extract actinides: acetamide phosphonate (Ac-phos), propionamide phosphonate (Prop-phos) and 1,2-hydroxypiridinone (HOPO) (Scheme 1). These three ligands were indeed shown to be promising for the capture of actinides when grafted on SBA-15 materials [2, 11, 20]. Their behavior under irradiation was then followed in detail, and the evolution of their sorption ability was studied as a function of the irradiation dose.

2. Materials and methods

2.1. Reagents

Potassium bromide (KBr, FT-IR grade) was purchased from Sigma Aldrich. Mohr salt ($(NH_4)_2Fe(SO_4)_2$, >99%) was obtained from Labosi, sulfuric acid (H_2SO_4, 99.999%) and sodium chloride (NaCl, >99%) were purchased from Merck and HNO_3 (69.5% purity) from Carlo Erba.

Argon (Ar, 99.9999%) was purchased from Air Products. De-ionized water (18.2 MΩ·cm) was obtained from a Millipore apparatus. All reagents were used without any further purification.

2.2. Synthesis of the grafted silicas

Grafted silicas (see Scheme 1) were synthesized according to previously reported procedures ([2, 11]). The synthesis of the ligands and of the various silicas is described in detail in the Supplementary Material. The 1,2-HOPO ligand (1,6-dihydro-6-oxo-N-[(triethoxysilyl)propyl]-2-carboxamide) possesses an amide group linked to a pyridine heterocycle containing C=O and N-OH groups. This compound is considered as aromatic since the lone pair on the nitrogen atom participates to electron delocalization [34]. The Ac-phos ligand ([2-oxo-2-((3-(triethoxysilyl)propyl)amino)ethyl]phosphonic acid) has a phosphonic acid functional group linked to an amide through a carbon atom. The Prop-phos ligand ([3-oxo-3-((3-(triethoxysilyl)propyl)amino)propyl]phosphonic acid) is similar to Ac-phos but contains one additional carbon between the amide and the phosphonic acid groups. All ligands are linked to the silicon atom through the amide and an alkyl chain containing three carbon atoms (see SI). The structures of the grafted mesoporous silicas and of their corresponding ligands (prior to their grafting) are shown in Scheme 1.

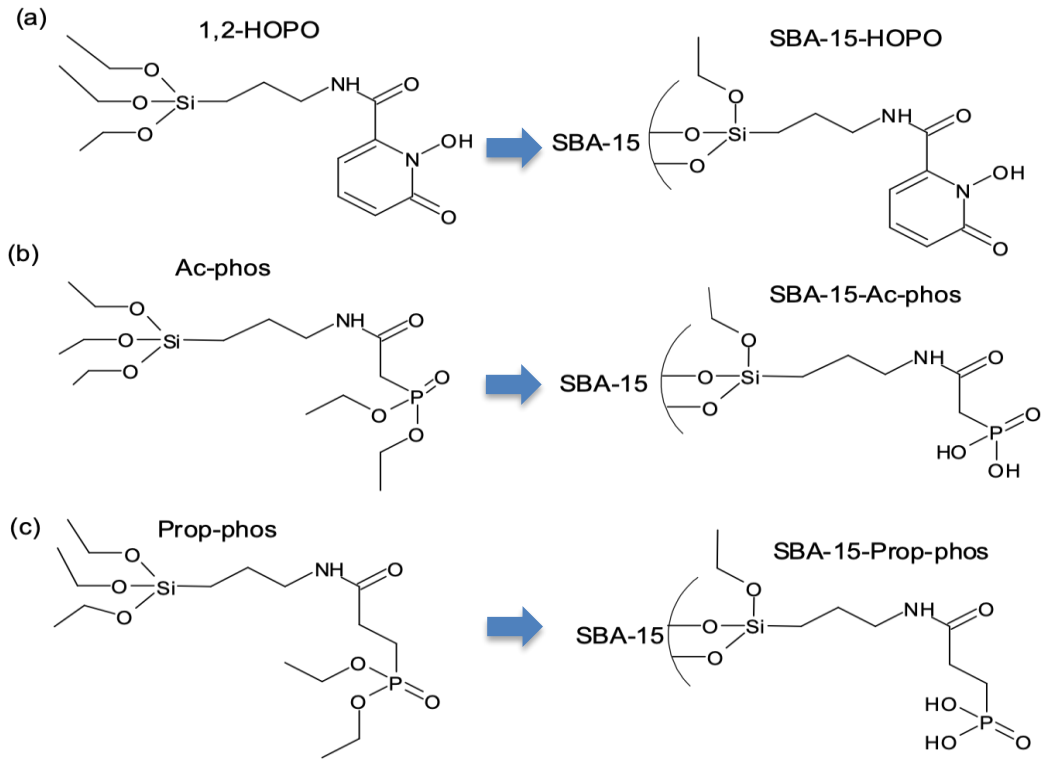

Scheme 1. *Structure of the grafted mesoporous silicas and the starting ligands. (a): 1,2-HOPO ligand*

(left) and SBA-15-HOPO (right); (b): Ac-phos ligand (left) and SBA-15-Ac-phos (right); (c): Prop-phos ligand (left) and SBA-15-Prop-phos (right)

2.3. Thermal treatment

All SBA-15 materials (grafted or not) were thermally treated in order to remove adsorbed water molecules. Pristine SBA-15 was heated at 400°C under vacuum (around 1 mbar) for 4 hours. Grafted SBA-15 was heated at 80°C under vacuum (around 1 mbar) for 24 hours. This temperature was chosen to avoid any damage to the grafted ligands.

2.4. Irradiation with 10 MeV electrons

Irradiation experiments were carried out with a Titan Beta, Inc. linear accelerator delivering high-energy electrons. 10 ns pulses of 10 MeV electrons at a repetition rate of 5 Hz were delivered to the samples. This frequency was chosen to avoid any sample heating. Around 300 mg of each sample was placed in a Pyrex ampule for analysis. In the case of the pure ligands, which are liquid at ambient temperature, argon was firstly bubbled for 30 minutes in order to remove dioxygen. Ampules were outgassed and filled with ultra-pure argon (99.9999%) three times prior to irradiation.

Fricke dosimetry [35] was used to estimate the dose delivered to the sample. It was determined to be 15 ± 2 Gy·pulse^{-1} (1 Gy = 1 J·kg^{-1}). The dose received by the Fricke solution was considered to be the same as the dose received by the sample [31].

2.5. FT-IR spectroscopy

The infrared (IR) spectra of the samples were recorded under vacuum (1 mbar) with a Brucker Vertex 80v FT-IR apparatus. 1 wt% of the sample was dispersed in high purity KBr, then pelletized into self-supporting discs using a pressure of 10^9 Pa. Spectra were then recorded from 400 scans in the 700-4000 cm^{-1} wavenumber range at a 2 cm^{-1} resolution. The KBr background was subtracted in all cases.

2.6. XPS

X-ray photoelectron spectroscopy (XPS) was performed with a hemispheric analyzer Kratos Analytical Axis Ultra DLD spectrometer, using an Al Kα source monochromatized at 1486.6 eV and a charge compensation system. A pass energy of 160 eV was used for the survey spectra

and of 20 eV for core levels measurements. The energy resolution of the source and of the analyzer was found to be 0.35 eV. A thin layer of the sample was deposited on a copper tape. In all cases, the carbon C 1s line at 284.8 eV was used as a reference to calibrate the binding energy. Data acquisition and processing were carried out using the Casa XPS processing software. After calibration, the background from each spectrum was subtracted using a Tougaard-type background.

2.7. Gas chromatography measurements

H_2, CO_2, CO and CH_4 produced under irradiation were quantified by micro gas chromatography (µ-GC) using an SRA Instrument µGC-R3000 apparatus, with argon as the carrier gas. If other gases than the above mentioned ones were produced, then they were identified by gas chromatography coupled to mass spectrometry (GC-MS) using an Agilent 6890 GC system and an Agilent 5977 MS system equipped with an electron impact (EI) source and a quadrupole mass analyzer. In this case, helium was the carrier gas and was used at a flow of 2 mL·min^{-1}. Separation was performed in split mode using a PorabondQ (25 m × 0.32 mm) column (Agilent) and a molecular sieve CP-Molsieve 5 Å (25m x 0.32 mm, Agilent). The temperature of the injector was set at 110°C.

2.8. Determination of grafting density

The grafting density ρ (expressed in groups·nm^{-2}) was calculated according to equation (1):

$$\rho = \frac{N_A \times (\%C)}{(C)_{grafted\ group}} \frac{10^{-18}}{(100-(\%C)) \times S_{BET}} \qquad (1)$$

where (%C) is the carbon percent of the sample obtained by combustion on an Elementar Vario Micro Cube CHNS/O Elemental Analyzer, N_A is Avogadro's constant, $(C)_{grafted\ group}$ is the molecular weight of carbon in the grafted group (g·mol^{-1}) and S_{BET} is the Brunauer–Emmett–Teller (BET) specific surface area of the SBA-15 before grafting (m^2·g^{-1}). Adsorption and desorption isotherms with nitrogen at 77 K were obtained using a Micromeritics Tristar unit (USA) for BET analysis. Before measurements, samples were degassed for 12 hours at 473 K and 373 K for pristine SBA-15 and grafted materials, respectively. BET surface area was estimated at a relative pressure lower than 0.25. The pore size distribution was obtained with the desorption isotherm curve using the Barrett-Joyner-Halenda (BJH) model. The results of these analyses for all the materials used in this study are given in Table 1.

Table 1. *Characteristics of the grafted materials used in this study*

Sample	Pore diameter before/after grafting (Å)	S_{BET} before/after grafting ($m^2 \cdot g^{-1}$)	%C	Grafting density (groups·nm^{-2})
SBA-15-HOPO	70/56	760/313	9.42	0.76
SBA-15-Ac-phos	65/55	766/318	9.68	1.4
SBA-15-Prop-phos	73/60	810/289	10.47	1.2

After grafting, the specific surface of the materials was found to be similar (around 300 $m^2 \cdot g^{-1}$), whatever the ligand grafted. The grafting density was found to be 0.76 groups·nm^{-2} for SBA-15-HOPO, 1.4 groups·nm^{-2} for SBA-15-Ac-phos and 1.2 groups·nm^{-2} for SBA-15-Prop-phos. These values are consistent with the commonly found grafting density of about 1 group·nm^{-2} in SBA-15 materials [36]. The grafting of the materials was further confirmed by means of XPS (Figure S1), FT-IR (Figure S2 together with the assignment of the characteristic bands in Table S1) and TGA (Figure S3). Moreover, the thermal treatment was shown not to damage the ligands, as evidenced in Figures S3 and S4 in the Supplementary Material, by TGA and FT-IR, respectively.

Notably, most of the grafted molecules are expected to be located within the porous structure of the silica since there is much less external surface area than internal area.

2.9. Sorption experiments

Aqueous solutions of thorium were prepared by dissolving the corresponding certified standard solution (SCP Science, 10 040 ± 50 µg.mL^{-1} in 4% HNO_3) of Th (IV) in deionized water. The pH of the solution was adjusted to 2.0 using HNO_3 (69.5% purity, purchased from Carlo Erba) and checked with a Mettler Toledo Seven Excellence pH-meter. 10 mg of the adsorbent was added to 20 mL of the solution. The mixture was then stirred at 200 rpm using a Heidolph

Rotamax 120 apparatus for at least 24 hours to ensure that the equilibrium was reached. Thorium initial (C_i, mg·L^{-1}) and equilibrium (C_e, mg·L^{-1}) concentrations in the solution were determined by X-ray fluorescence using a Xeros EDX RF apparatus. This allowed calculating the equilibrium sorption capacity (q_e, mg·g^{1}) using equation (2) [7]:

$$q_e = \frac{C_i - C_e}{m} \times V \quad (2)$$

where m is the mass of adsorbent (g) and V is the volume of the aqueous solution (L).

3. Results and discussion

3.1. Behavior of ligands under irradiation

3.1.1. Gas production under irradiation

The amount of gas produced under irradiation enables both the estimation of the extent of damage undergone by the molecule. The nature of the produced gases also enables the identification of the particular bonds that were damaged. µ-gas chromatography was used to quantify H_2, CO, CO_2 and CH_4 produced during irradiation of the three ligands. The corresponding gas production plots as a function of the dose are shown in Figure 1.

The production of gases increased linearly with the dose (Figure 1). The slope of each curve corresponds to the radiolytic yield of each gas [37], which are given in Table S2 in the Supplementary Material for all three molecules and are also shown in Figure 1d.

For all three molecules, the major gas produced was H_2, which can be attributed to the cleavage of C-H and N-H bonds, as well as of the O-H bond in 1,2-HOPO molecules. Although Ac-phos and Prop-phos differ by one -CH_2-, they exhibited the same H_2 radiolytic yield (1.6 x 10^{-1} µmol·J^{-1}). It is on the same order of magnitude as the H_2 radiolytic yield measured in linear saturated alkanes in the liquid state (around 5×10^{-1} µmol·J^{-1} for pentane and hexane for example, [38]), which highlights the efficient radiolytic H_2 production of these two molecules. Gas production under irradiation was slighlty higher for Prop-phos than for Ac-phos, due to the higher CO and CO_2 production of the former sample. In contrast, the 1,2-HOPO molecule produced significantly less gas under irradiation, independent of the gas considered, with a total gas production 20 times lower than for the two other ligands. This can be attributed to the presence of the aromatic ring, which has a radioprotector effect [38]. For all three molecules, CO_2 and CH_4 were produced in lower amounts than H_2. CO was detected during

irradiation of Ac-phos and Prop-phos only. The low production of these gases evidences that the corresponding pathways are less important to radiation damage than the H_2 production mechanisms.

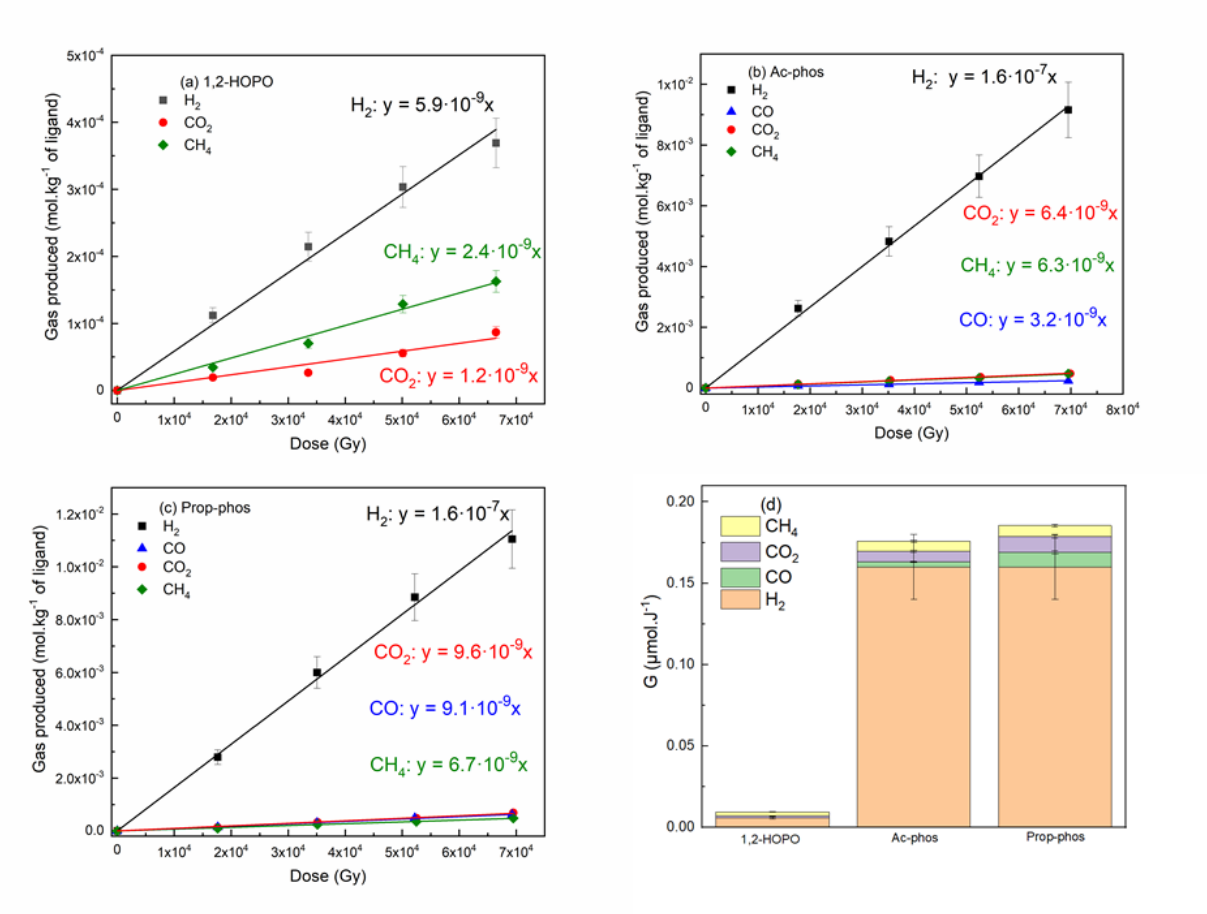

Figure 1. *Evolution of H_2, CO, CO_2 and CH_4 production (in mol·kg^{-1} of material) as a function of the irradiation dose (Gy) for (a) 1,2-HOPO, (b) Ac-phos and (c) Prop-phos ligands. (d) Radiolytic yields of the gases produced under irradiation from the three starting ligands. A magnification of the CO, CO_2 and CH_4 curves of Ac-phos and Prop-phos is displayed in the Supplementary Material (Figure S5). The lines are linear fits to the data. The slopes of the lines are given for each case.*

GC-MS experiments were also performed in order to identify any other gases produced during irradiation of the three ligands. The corresponding chromatograms of the samples irradiated at 100 kGy are shown in Figure 2. As no gas was detected in the pristine samples, the gas displayed below are due to irradiation only.

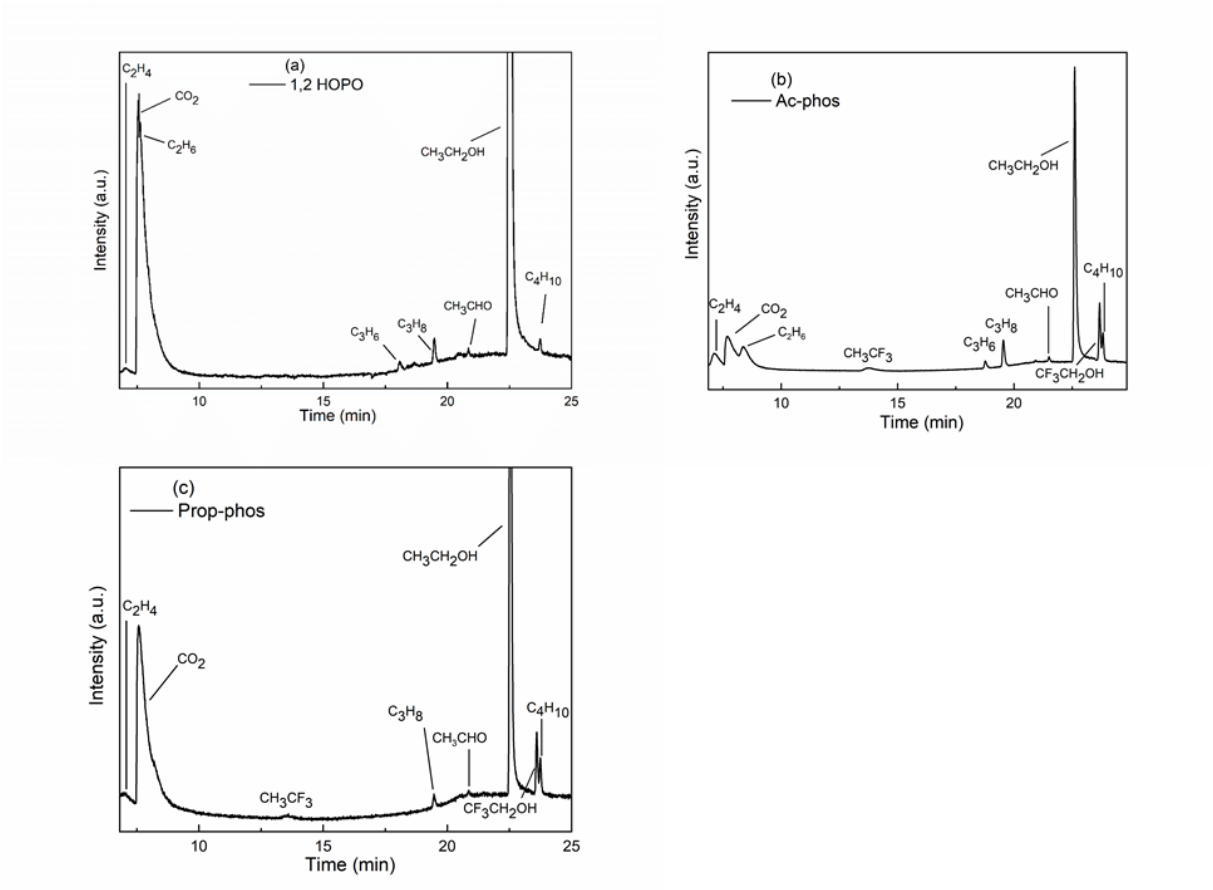

Figure 2. *Gas degradation products of (a) 1,2-HOPO, (b) Ac-phos and (c) Prop-phos ligands measured by GC-MS after a 100 kGy radiation dose. No gas was detected in the non-irradiated samples. Magnification is applied on graphs (a) and (c) and the peak attributed to ethanol is not shown entirely.*

Notably, the same molecules were detected in all cases. Thus, the formation of C_2H_4, C_2H_6, C_3H_6, C_3H_8 and C_4H_{10} (Figure 2) attests that alkanes and alkenes were produced under irradiation. C_2H_4 may be formed as a result of the subsequent irradiation of C_2H_6. Together with the production of CH_4, the production of alkanes/alkenes is a clear signature of C-C bond rupture. Traces of fluorinated impurities such as CF_3CH_2OH and CH_3CF_3 are detected on the chromatograms and are attributed to the use of fluorinated compounds during the synthesis [20]. CH_3CH_2OH (ethanol) and CH_3CHO (ethanal) were also detected. We checked carefully that ethanol was not a pollutant due to the cleaning procedure, and thus confirmed that it was produced in significant amounts during the irradiation of the ligands. The cleavage of Si-O or P-O bonds could explain the production of these latter gases, however, the production of ethanol was observed in irradiated 1,2-HOPO despite the absence of P-O bonds. Therefore, ethanol production most likely resulted from the cleavage of Si-O bonds. Ethanal production may have been the result of the irradiation of ethanol [38].

3.1.2. Reaction mechanisms in irradiated ligand molecules

Gas production also provides insight into the degradation mechanisms of molecules under irradiation. The production of ethanol indicates that irradiation modifies the molecule near the silicon atom. Upon irradiation, the energy deposited in the sample (*M*) leads to the production of a radical cation ($M^{\bullet+}$), an electron (e^-) and an excited molecule (*M**) according to reaction R1:

$$M \xrightarrow{Ionizing Radiation} M^{+\bullet} + e^-, M^* \qquad \text{R1}$$

The electron can then solvate. Even if some physical parameters such as the dielectric constant of these liquids are not known – making a precise description of phenomena difficult – the significant ethanol formation detected on chromatograms (Figure 2) for all cases suggests the cleavage of the Si-O bonds. Cleavage of Si-O bonds leads to the production of $R_1(R_2)_2Si^\bullet$ radicals. Notably, the ATR spectrum of the HOPO ligand (displayed in Figure S6a) shows a clear loss of CH_3 bonds as well as an increase in O-H bonds after irradiation. The ATR spectra of Ac-phos and Prop-phos ligands (Figure S6b and Figure S6c) also show features of the loss of Si-OC_2H_5 groups. This can be explained by the formation of silanol groups. Indeed, radicals can readily react with traces of water to produce silanols and $H^\bullet$ radicals, according to reaction R2:

$$(CH_3CH_2O)_2Si^\bullet - R + H_2O \xrightarrow{Ionizing\ radiation} R(CH_3CH_2O)_2Si - OH + H^\bullet \qquad \text{R2}$$

$H^\bullet$ species can for instance dimerize into H_2 according to R3:

$$H^\bullet + H^\bullet \rightarrow H_2 \qquad \text{R3}$$

Another H_2 source consists of an $H^\bullet$ atom abstraction from the grafted molecule by the hydrogen atom [38].

Notably, H atoms are linked to carbon or nitrogen atoms in the molecules under study. The cleavage of C-H bonds on the alkyl chain was observed during the radiolysis of different amide molecules [39]. In addition, the radiolysis of dry alkyl amines showed that the cleavage of N-H bonds was preferred over that of C-H bonds [40]. This suggests that both bonds are cleft under ionizing radiation, and that the breakage of the N-H bond may be the preferential one.

Other gases are produced in smaller quantities than H_2. Among them, the production of CH_4 as well as of other alkanes detected by GC-MS is a clear sign of C-C bond cleavage on the alkyl chain of the molecules [37]. CO and CO_2 could be formed after the breakage of (O=)C-C and N-(C=O) bonds, which are likely to be cleft, as reported in the radiolysis of amides and diamides [41-47].

3.2. Behavior of grafted materials under irradiation

3.2.1. Gas production under irradiation

The degradation of the pristine and of the grafted SBA-15 materials under irradiation was studied by micro-chromatography in order to determine the radiolytic production of H_2, CO and CO_2. No CH_4 was detected in any case. The evolution of the amount of these gases is plotted as a function of the dose for the three samples in Figure 3.

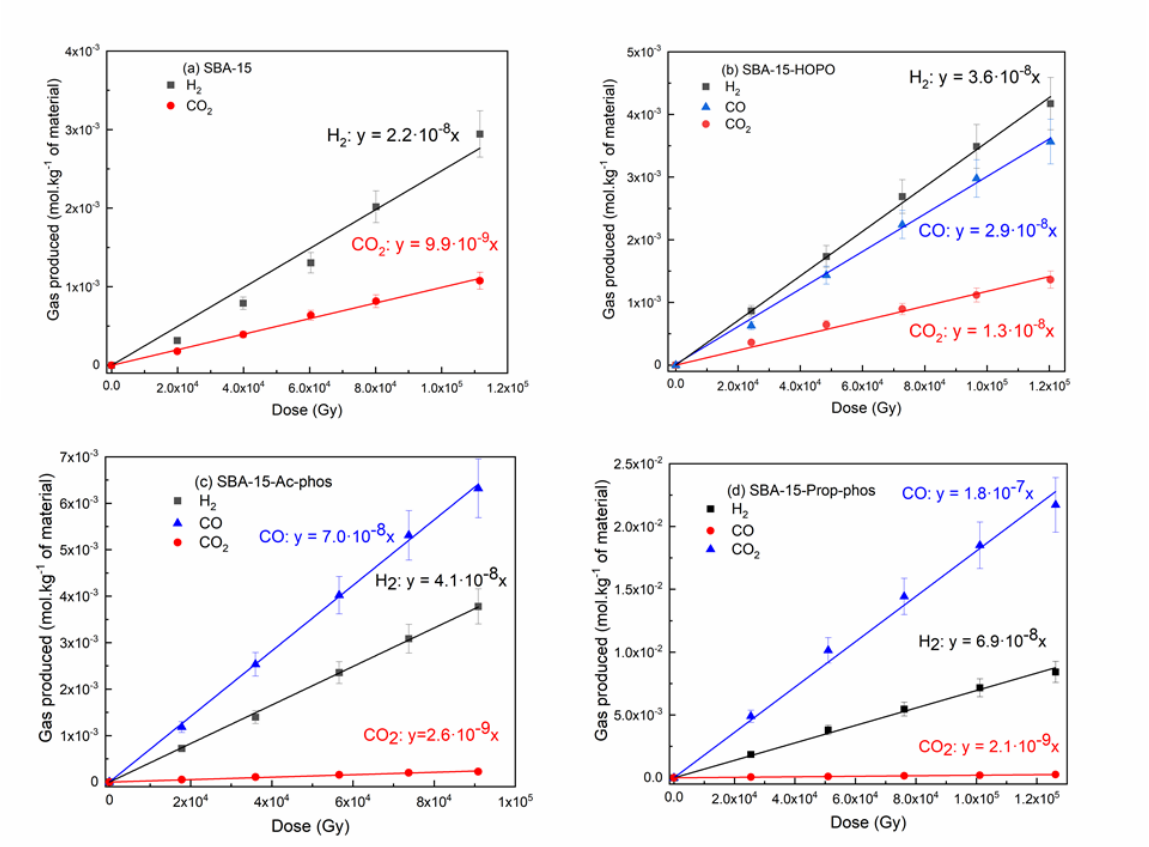

Figure 3. *Evolution of H_2, CO and CO_2 (in mol·kg^{-1} of material) production under irradiation as a function of the cumulated dose (Gy) for (a) pristine SBA-15, (b) SBA-15-HOPO, (c) SBA-15-Ac-phos and (d) SBA-15-Prop-phos. All samples were thermally treated prior to irradiation.*

For all samples, the amount of gases produced evolved linearly with the dose, allowing the measurement of the radiolytic yield from the slope of the line (G, mol·J^{-1}) for each gas. The

various radiolytic yields measured are given in Table S4. The radiolytic yields of the irradiated grafted SBA-15 materials are displayed for the purpose of comparison in Figure 4.

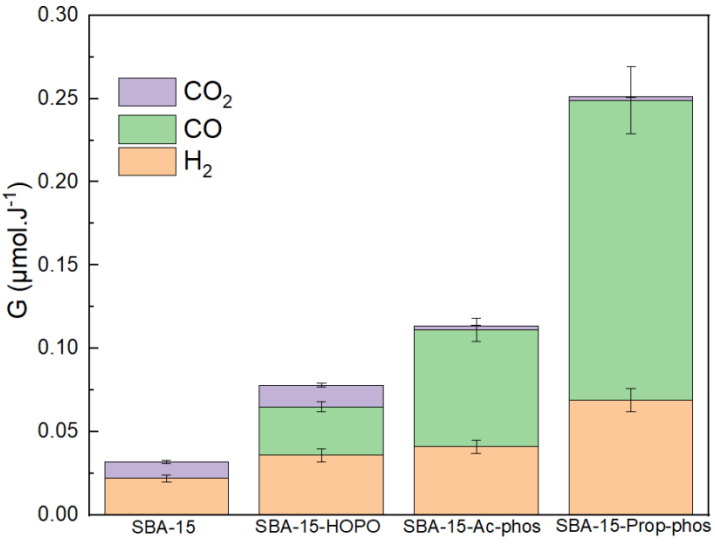

Figure 4. *Radiolytic yields of the gases produced under irradiation from the various systems under study.*

For pristine SBA-15, the only gases produced are H_2 and CO_2, as evidenced by complementary GC-MS measurements. The formation of carbon dioxide was probably due to the radiolysis of residual ethoxy groups in the SBA-15 matrix [48]. Compared to pristine SBA-15, the three grafted materials show a similarly low production of CO_2, with radiolytic yields within the same order of magnitude, or even lower. This suggests that the origin of the carbon dioxide production is the same in all samples, and it may be attributed to the radiolysis of residual ethoxy groups. For all samples, CH_4 was never detected, indicating that C-C bond cleavage is not a significant reaction pathway.

The H_2 radiolytic yield is slightly higher for the grafted SBA-15 samples than for the pristine one. The H_2 production arises from the radiolysis of water and silanols [31] as well as from the grafted ligand. Thus, the radiolysis of the alkyl chain of the ligand can account for the higher H_2 production as compared to the pristine sample.

The CO and H_2 radiolytic yields increase proportionally in the following order according to the nature of the grafting: HOPO < Ac-phos < Prop-phos, which suggests that ligands with more alkyl carbons are more likely to produce CO and H_2. The H_2 radiolytic yield is lower for SBA-15-HOPO, confirming the effect of the aromatic ring as an efficient radioprotector [38]. However,

the grafting density is also lower in SBA-15-HOPO than in the two other materials (Table 1). Of course, even if the difference in grafting density does not by itself explain the large difference in quantities of gas produced between SBA-15-HOPO and the other samples, it must help to explain part of the observed decrease. We note that the protective effect of the aromatic ring seems to be lower for grafted SBA-15 than for the neat ligand. Indeed, under irradiation, the total number of (CO, CO_2, H_2 and CH_4 molecules, if present) produced from SBA-15-HOPO ((7.8 ± 0.8) x 10^{-2} µmol·J^{-1}) is significantly higher than from the 1,2-HOPO ligand ((9.4 ± 0.9) x 10^{-3} µmol·J^{-1}).

Since CO is not formed during irradiation of the pristine silica, its production arises from the irradiation of the grafted ligands. As it is generated in all grafted materials, with the SBA-15-HOPO showing the lowest CO radiolytic yield in spite of its two C=O bonds, this gas most likely comes from the lysis of the C=O of the amide group on the alkyl chain of the ligands.

Notably, the radiolytic yields measured for the grafted SBA-15 samples show different gas production from that of the starting ligands, both in terms of quantity and of gas distribution. For the ligands, the main gas produced is H_2, accompanied by a minor production of CO, CO_2 and CH_4. For the grafted SBA-15 samples, the main gas produced is CO, except in the case of SBA-15-HOPO, indicating that the same molecules behave differently under irradiation depending on whether they are grafted on SBA-15 or not. The total amount of these produced gases is higher for the grafted SBA-15 samples than for the ligands, which is another evidence of the difference of behavior under irradiation.

GC-MS analysis of the gases produced upon a 100 kGy radiation dose of the grafted materials was also performed (Figure 5).

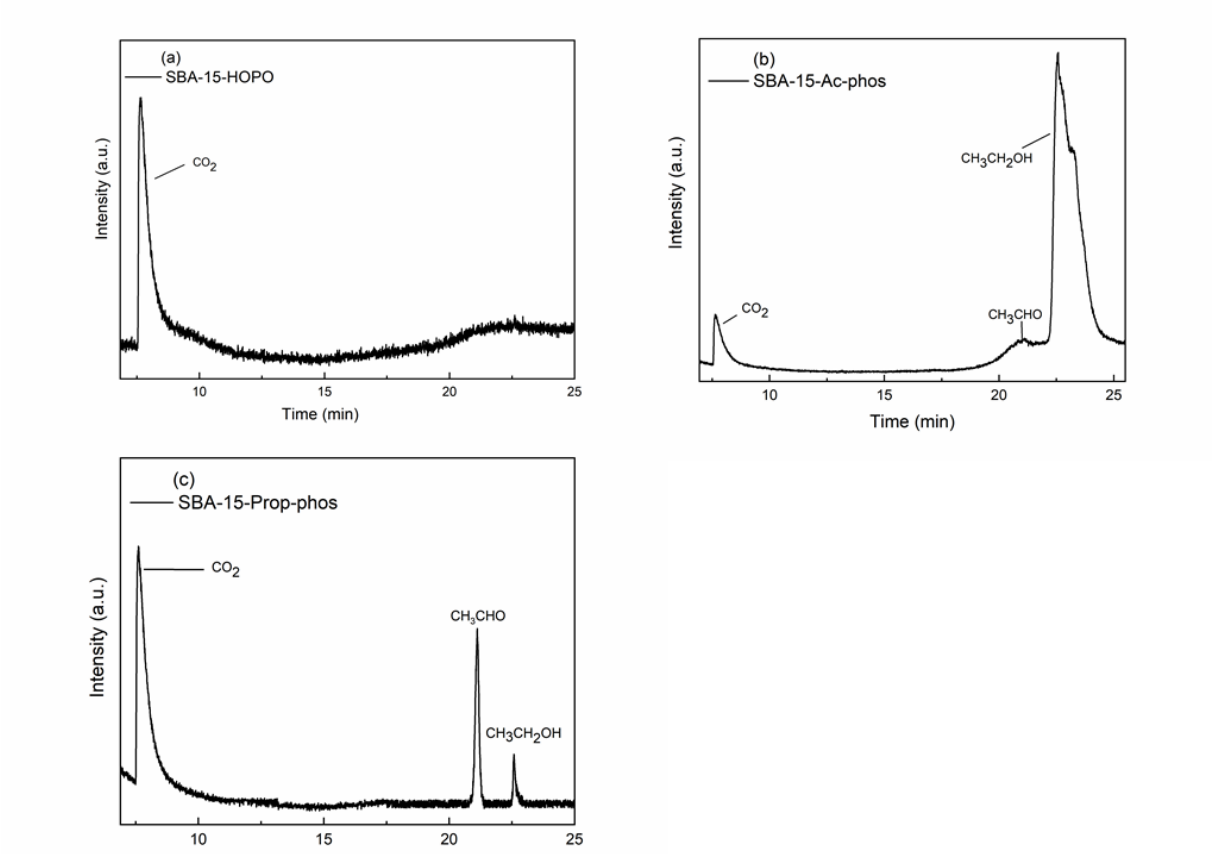

Figure 5. *Gas decomposition products of the grafted (a) SBA-15-HOPO, (b) SBA-15-Ac-phos and (c) SBA-15-Prop-phos ligands measured by GC-MS after a 100 kGy radiation dose. No gas was detected in the non-irradiated samples.*

GC-MS analysis of the gases produced upon irradiation confirms that the cleavage of C-C bonds in the grafted SBA-15 samples is not likely to occur. Indeed, no alkanes were detected on the chromatograms, in contrast with the various alkanes/alkenes detected after irradiation of the ligands. Notably, the number of different gases produced is rather low, indicating that there are preferential reaction channels. For the SBA-15-HOPO material (as well as for the pristine SBA-15), no gases other than CO_2 were detected, confirming the protective role of the aromatic ring towards the decomposition of the ligand. For the two other samples, ethanol (CH_3CH_2OH) and CH_3CHO were produced. Notably, these compounds were also formed in the irradiated ligands. As in the case of the ligand molecules, their formation cannot be attributed to pollution due to cleaning. Moreover, as for the ligands, these compounds can arise from the cleavage of the Si-O bond in the grafted ligand. Another gas was detected as a shoulder on the SBA-15-Ac-phos sample, with a retention time of about 23 minutes. Unfortunately, it was not possible to assign it precisely.

3.2.2. Characterization of the materials before and after irradiation

The evolution of the samples before and after irradiation of 0.5 MGy and 4 MGy was assessed by FT-IR spectroscopy (Figure S7; with a magnification of the 1300-1750 cm^{-1} wavenumber region, which is the region of interest where changes can be evidenced, in Figure 6; see also the assignment of the infrared bands in Table S1). Notably, higher doses were used for spectroscopy experiments than for gas measurements. Indeed, the sensitivity of these latter experiments is here much higher than that of *ex situ* spectroscopy. The bands related to the SBA-15 matrix at 800 cm^{-1} and 1080 cm^{-1} did not evolve after irradiation. Similarly, the characteristic bands of the ligands were almost unaffected after irradiation at 500 kGy. However, modifications were detected when samples were irradiated at 4 MGy.

For all samples, the CH_2 stretching bands of the grafted ligands (detected around 2940 cm^{-1}) had a lower intensity after irradiation at 4 MGy, which is a consequence of C-H bond cleavage (Figure S7). Clearly, the intensity of the broad band in the 3000-4000 cm^{-1} region decreased, indicating a decrease in the O-H content of the samples after irradiation (Figure S7, [49]). The modification of the shape of this band indicates the radiolysis of residual water as well as of the SiO-H bond. Moreover, the cleavage of N-H bonds is also evidenced by the lower intensity of the bands located around 3100 cm^{-1} and 3280 cm^{-1}.

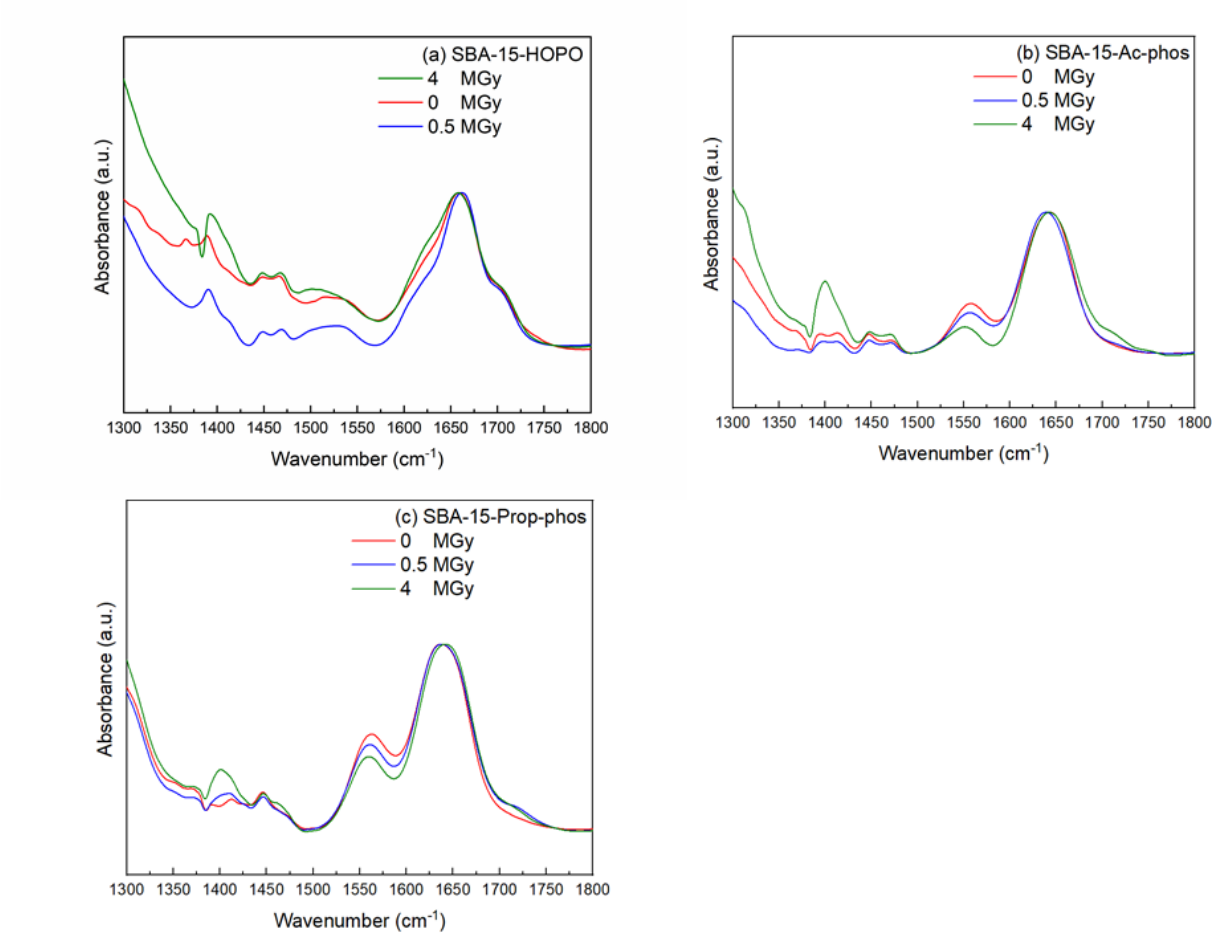

Figure 6. *FT-IR spectra of grafted SBA-15 unirradiated and irradiated at 0.5 MGy and 4 MGy: (a) SBA-15-HOPO; (b) SBA-15-Ac-phos; (c) SBA-15-Prop-phos. The spectra are shown in the 1300-1750 cm^{-1} wavenumber range and normalized with respect to the C=O stretching mode at 1660 cm^{-1}. The spectra were recorded under vacuum.*

In the 1300-1750 cm^{-1} wavenumber range, the characteristic absorption bands of the grafted HOPO ligand such as the C=O stretching band at 1640 cm^{-1} appear to be barely modified upon irradiation (Figure 6a). In contrast, the characteristic bands in the 1500-1800 cm^{-1} wavenumber range of the Ac-phos (Figure 6b) and Prop-phos (Figure 6c) ligands evidence modifications upon irradiation. The C=O and NH vibration bands are still observed around 1650 cm^{-1} and 1570 cm^{-1}, respectively, but with a lower intensity than in the un-irradiated materials as evidenced by the spectra obtained after normalization to the silica matrix bands (Figure S7, especially for Ac-phos). Concomitantly, a vibrational band at around 1720 cm^{-1} appears after irradiation (Figure 6b and 6c). It can be attributed to a C=O stretching vibration of an aldehyde or of an acid [49]. Indeed, the formation of an amic acid with a N-COOH functional group could be responsible for the band at 1720 cm^{-1} [50]. Moreover, the appearance of a peak at around

1400 cm^{-1} could also be due to an in-plane O-H deformation vibration characteristic of an amic acid [49, 51]. Notably, the same is observed for SBA-15-HOPO (Figure 6a), but with a much weaker intensity. In conclusion, we suggest that an amic acid group is formed upon irradiation of these grafted samples. However, an aldehyde might also be produced. The formation of an aldehyde group should be accompanied by the formation of an amine (see Scheme 1 with the various chemical structures under study), although we did not detect an amine by FT-IR (discussed below).

XPS analysis of the materials before and after irradiation gives a further insight into the modifications at the surface of the materials. The N1s spectra are shown in Figure 7.

Two contributions are present before irradiation. The first one, located at 400.0 eV, corresponds to N-C=O bonds from an amide functional group. The second one is located at 401.9 eV and is attributed to "N^{+}"-type species [52]. In this case, this labelling implies a hydrogen-bonded nitrogen atom. Here, it is assigned to the N-H contribution. The hydrogen bonds contribute to increase the positive charge on the nitrogen atom [52]. The nitrogen atom of the N-OH function found in the SBA-15-HOPO sample probably falls into this latter category.

In all cases, after irradiation, the proportion of the signal at 400.0 eV significantly decreased, and the proportion of the signal at 401.9 eV increased. This indicates that irradiation decreases the contribution of the N-C=O groups while increasing the number of N-H bonds. Interestingly, this change in the relative proportion of both components is in the order: SBA-15-HOPO < SBA-15-Ac-phos < SBA-15-Prop-phos, i.e. in the same order as the measured CO (or total gas) production (see Figure 4). Moreover, the TGA curves of SBA-15-Ac-phos (shown in Figure S8) clearly show an additional region of mass loss as compared to un-irradiated SBA-15-Ac-phos. This extra mass loss could be attributed to the formation of an amine [53]. Amine formation was not observed on the IR spectra, but this could be attributed to a too weak signal to allow detection. Notably, the CO gas production implies the formation of an amine, which in turn would lead to the higher contribution of the "N^{+}" signal as confirmed by XPS spectroscopy. The amine formation should be accompanied by an aldehyde formation, as described above.

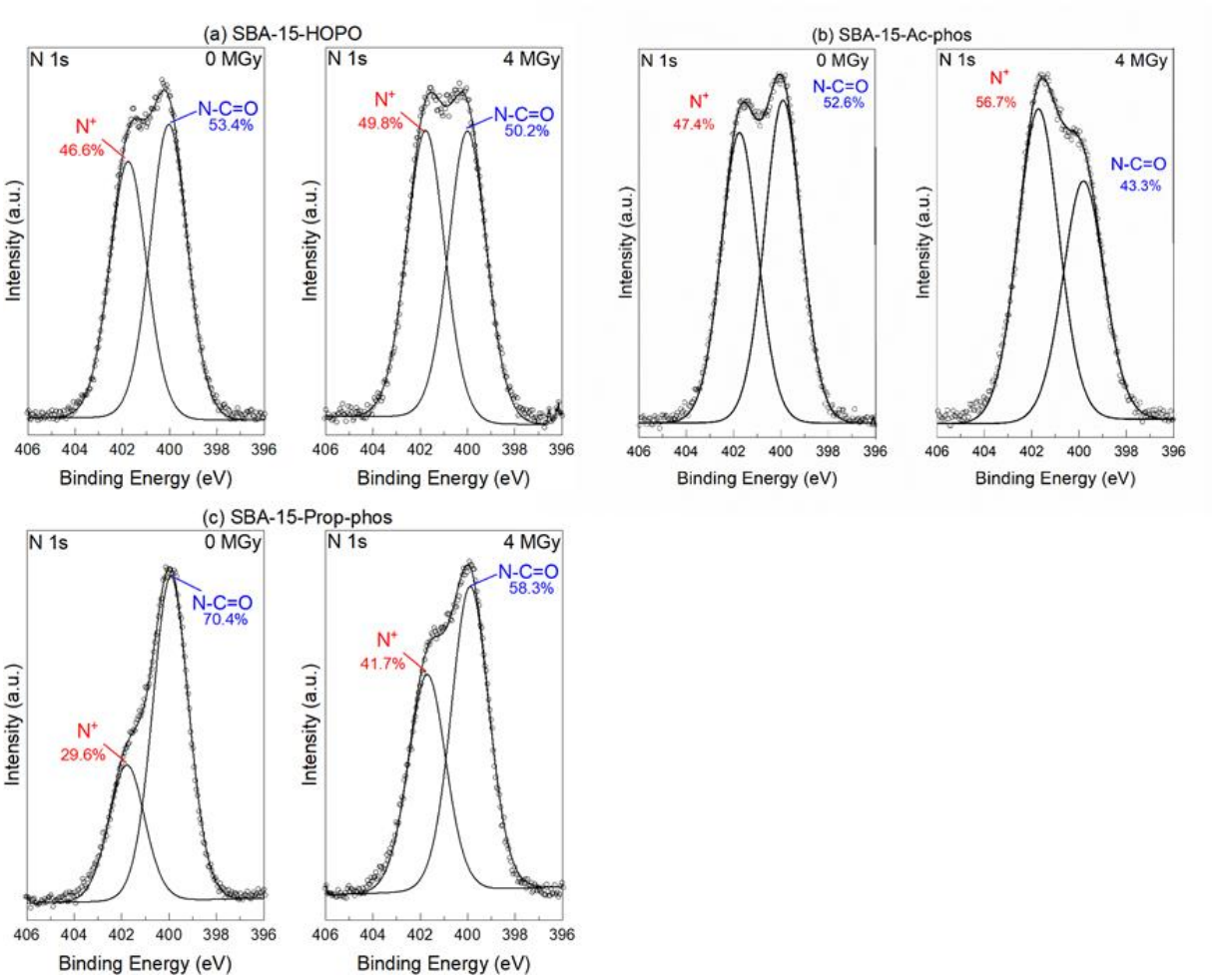

Figure 7. *N1s X-ray core-level spectra of non-irradiated samples (left) and samples irradiated at 4 MGy (right). Experimental data are shown as circles, and the lines are the corresponding fits to the data. (a) SBA-15-HOPO, (b) SBA-15-Ac-phos and (c) SBA-15-Prop-phos. SBA-15 is not shown, as it does not contain nitrogen atoms (see also Figure S1 in the Supplementary Material).*

The behavior of the environment around phosphorus atoms can be assessed through XPS core-level spectra of P 2p (see Figure S9 for SBA-15-Ac-phos and SBA-15-Prop-phos samples). Two contributions are evidenced on these spectra. The first one, located at 133.7 eV, corresponds to a P=O bond, while the second one corresponds to O-P=O groups, and is located at 134.7 eV [7]. The comparison of the spectra measured for the samples before and after irradiation at 4 MGy evidences that the phosphinic acid group is not modified upon irradiation. This result suggests that the amide group is more likely to be cleft upon irradiation than the phosphinic acid group. This is in line with a previous study on the irradiation of CMPO molecules [46], possessing both an amide and a phosphine oxide group. In this case, the amide group was shown to be preferentially cleft upon irradiation. The C 1s core-level spectra of

SBA-15-HOPO, SBA-15-Ac-phos and SBA-15-Prop-phos before and after irradiation are displayed in Figure 8.

Four different contributions are detected on the C1s spectra: (i) C-C and C-H bonds at 284.8 eV, (ii) (O=C)-C and C-N bonds at 285.8 eV, (iii) C-O bonds at 286.8 eV and (iv) N-C=O bonds at 288.4 eV. A fifth (v) contribution is found for SBA-15-HOPO at 287.9 eV, which corresponds to the ketone on the aromatic ring [50, 54].

After irradiation, the contribution (i) at 284.8 eV is generally slightly modified due to C-H bonds cleavages and other modifications in the grafting. The contribution (iv) at 288.4 eV clearly decreases after irradiation, indicating a loss of N-C=O bonds. This is due to the lysis of the amide group.

The cleavage of the Si-O bond contributes to the loss of O-C component, as attested by the lower (iii) signal obtained at 286.8 eV for SBA-15-Ac-phos and, more clearly, for SBA-15-Prop-phos. This contribution is higher for SBA-15-HOPO after irradiation due to the presence of a C-O bond on the aromatic ring, which is probably not cleft under irradiation. For the same reason, the C=O contribution (v) at 287.9 eV is also higher after irradiation than before for SBA-15-HOPO.

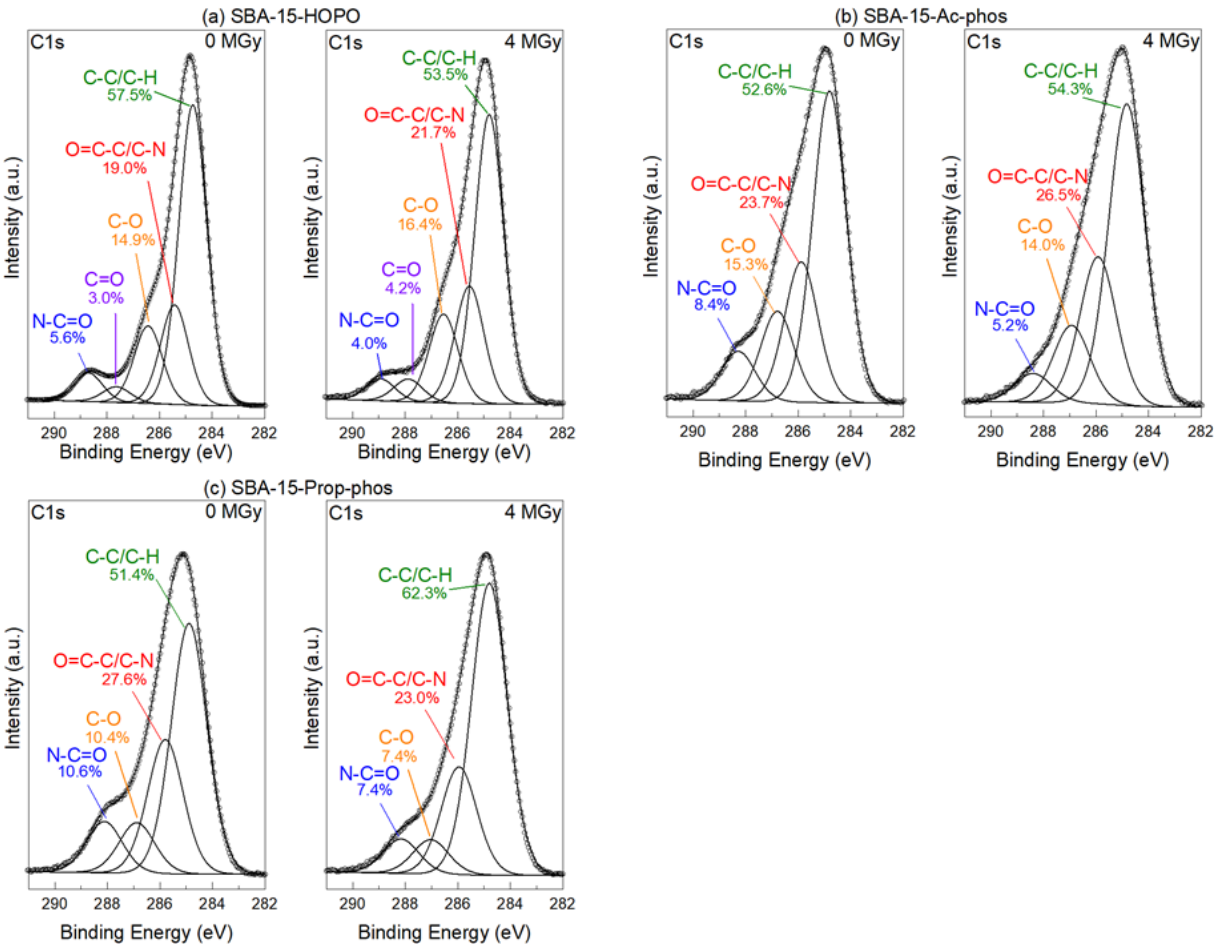

Figure 8. *C 1s X-ray core-level spectra of non-irradiated samples (left) and of samples irradiated at 4 MGy (right). Experimental data are circles, and lines are the corresponding fits to the data. (a): SBA-15-HOPO; (b): SBA-15-Ac-phos; (c): SBA-15-Prop-phos.*

The loss of C-N bonds under irradiation (signal (ii) at 285.8 eV) should lead to a decrease of this contribution. However, the signal at 285.8 eV could also be attributed to O=C-C bonds which can be formed upon irradiation (formation of amic acid and of aldehyde). Therefore, due to the interplay between these two effects, this contribution increases after irradiation as compared to before, in some cases (SBA-15-HOPO and SBA-15-Ac-phos), while it decreases in the third case (SBA-15-Prop-phos; Figure 8c).

3.2.3. Proposed degradation mechanisms of grafted SBA-15 materials

The experiments performed on the ligands and on the grafted materials clearly evidence that the proportions and amounts of gases produced under irradiation are significantly different, whether the ligand is grafted on the SBA-15 matrix or not. This implies different irradiation

mechanisms in both cases. Indeed, direct radiolysis affects the ligand molecules. However, in the case of grafted SBA-15 materials, the ligand represents less than roughly 20% of the mass of the material (as evidenced by TGA analysis; see Figure S3 in the Supplementary Material). Radiolysis will thus mainly affect the silica matrix. Electrons and holes are formed upon interactions between ionizing radiation and matter (R4):

$$SiO_2 \xrightarrow{IonizingRadiation} e^- + h^+ \qquad \text{R4}$$

Since the walls of the SBA-15 are thick, the electron-hole pairs can recombine to form excitons, according to the following reaction (R5):

$$e^- + h^+ \rightarrow {}^3excitons \qquad \text{R5}$$

These excitonic species are responsible for energy transfer processes at the surface of silica, allowing, for example, the cleavage of SiO-H bonds to form hydrogen radicals (R6). These excitonic species are responsible for the damage of the grafted ligands due to indirect radiolysis.

$$^3excitons + \equiv SiOH \rightarrow \equiv SiO^\bullet + H^\bullet \qquad \text{R6}$$

These hydrogen radicals can then dimerize to form H_2 according to reaction (R2) or abstract another hydrogen atom from the grafted molecule. Excitons lead also to homolytic bond cleavages on the ligand molecules as described in reaction R7:

$$^3excitons + R_1R_2C - H \rightarrow R_1R_2C^\bullet + H^\bullet \qquad \text{R7}$$

This reaction is possible with carbon or nitrogen atoms and creates carbo- or nitro-centered radicals ([36]), resulting in the formation of double bonds on the grafted molecules (an example is illustrated below, see bond cleavage (4) in Scheme 2).

However, the C-C bond breakage is more likely to occur in the non-grafted ligand, as evidenced from the production of CH_4 and alkanes (Figure 1), which was not observed during the irradiation of the grafted SBA-15 materials (Figure 4). According to the exciton theory, C-H bond excitons are preferentially localized in pairs of excitons, while C-C bond excitons migrate quickly between C-C bonds [55]. This exciton localization makes the breakage of C-H bonds more probable than C-C bond rupture, accounting for the fact that it is more observed in the grafted ligands than when pure ligands are exposed to ionizing radiation. Moreover, bond cleavage resulting from the production of excitons can be very specific to the nature of the bond. The model developed by Alam *et al*. [56] showed that a bond is likely to be cleft if the

bond dissociation energy is overlapped by the band gap value of the exciton. Both the silica matrix and the grafted layer act as an exciton propagation layer, leading to selective dissociation channels [29]. This phenomenon accounts for the fact that some degradation pathways are favored during the irradiation of grafted SBA-15 samples whereas it is not the case in the pure non-grafted ligand. Indeed, the cleavage of Si-O bonds (bond rupture 1 in Scheme 2) was evidenced by the production of ethanol (Figure 5). This bond cleavage is favored since the energy of the exciton (around 9 eV, approximated as the SiO_2 band energy, [57]) is very close to the bond dissociation energy of the Si-O bond (around 8 eV, [58]). Therefore, the energy transfer is near its resonance, probably leading to efficient processes (reaction R8).

$$^{3}excitons + (R_1)_2R_2Si - OCH_2CH_3 \rightarrow (R_1)_2R_2Si^{\bullet} + CH_3CH_2O^{\bullet} \quad \text{R8}$$

The $(R_1)_2R_2Si^{\bullet}$ radicals formed will then readily react with trace water molecules to form silanols [59], similarly to what is described in reaction (R1), as well as illustrated in Scheme 2, while the ethoxy radical will abstract one hydrogen atom, leading to the formation of ethanol. Notably, in SBA-15-HOPO, where the aromatic ring plays a protective effect towards ionizing radiation, no ethanol is detected

The production of CO from the lysis of the amide function is due to the cleavage of (O=)C-N and C-C(=O)N bonds, summarized by bond cleavages (2) and (3) on Scheme 2, respectively. Bond cleavage of the amide groups of malonamides was often reported [43, 39]. Notably, C-N bond dissociation is close to 8 eV [58]. Therefore, the preferential homolytic cleavage of this bond can be explained through the resonance effect of exciton theory. The energy of the other bonds is lower than 6 eV [58] making their cleavage less likely to occur. The (O=)C-N bond is probably first cleaved, and CO is released in a second step.

Notably, CO_2 was observed during the radiolysis of octyl(phenyl)-N,N-diisobutylcarbamoylmethyl phosphine oxide in the presence of water and oxygen (abbreviated as CMPO, [46]). CMPO degradation was initiated by C-N bond scissions, probably due to H abstraction of the nitrogen atom. This led to the formation of a carboxylic acid and an amine group (R9) [47]:

$$R_2(PO)CH_2(CO)NR_2 \overset{H_2O}{\rightarrow} R_2(PO)CH_2(CO)OH + HNR_2 \quad \text{R9}$$

with $R_2(PO)CH_2(CO)NR_2$ corresponding here to the CMPO molecule.

Further cleavage of the C-C(=O) bond produces CO_2, according to (R10):

$$R_2(PO)CH_2(CO)OH \rightarrow R_2(PO)CH_3 + CO_2 \qquad \text{R10}$$

In our case, rupture of the (O=)C-N bond is expected to lead to the formation of an amine and an aldehyde according to the following reaction (R11):

$$R_1(CO) - NHR_2 \overset{exciton}{\rightarrow} R_1CO^{\bullet} + HR_2N^{\bullet} \qquad \text{R11}$$

Both radicals will abstract hydrogen atoms to form R_1COH and R_2NH_2, R_1 being the phosphonate group linked to the amide and R_2 being the alkyl chain linked to the nitrogen atom.

Then, further degradation of the aldehyde leads to CO production, according to reaction R12:

$$R_1(COH) \rightarrow R_1H + CO \qquad \text{R12}$$

Even if it less probable, the rupture of the C-(CO) bond could lead to the production of an amic acid in the presence of trace water molecules (R13):

$$R_1(CO)NHR \overset{H_2O}{\rightarrow} R_1H + OH(CO)NHR \qquad \text{R13}$$

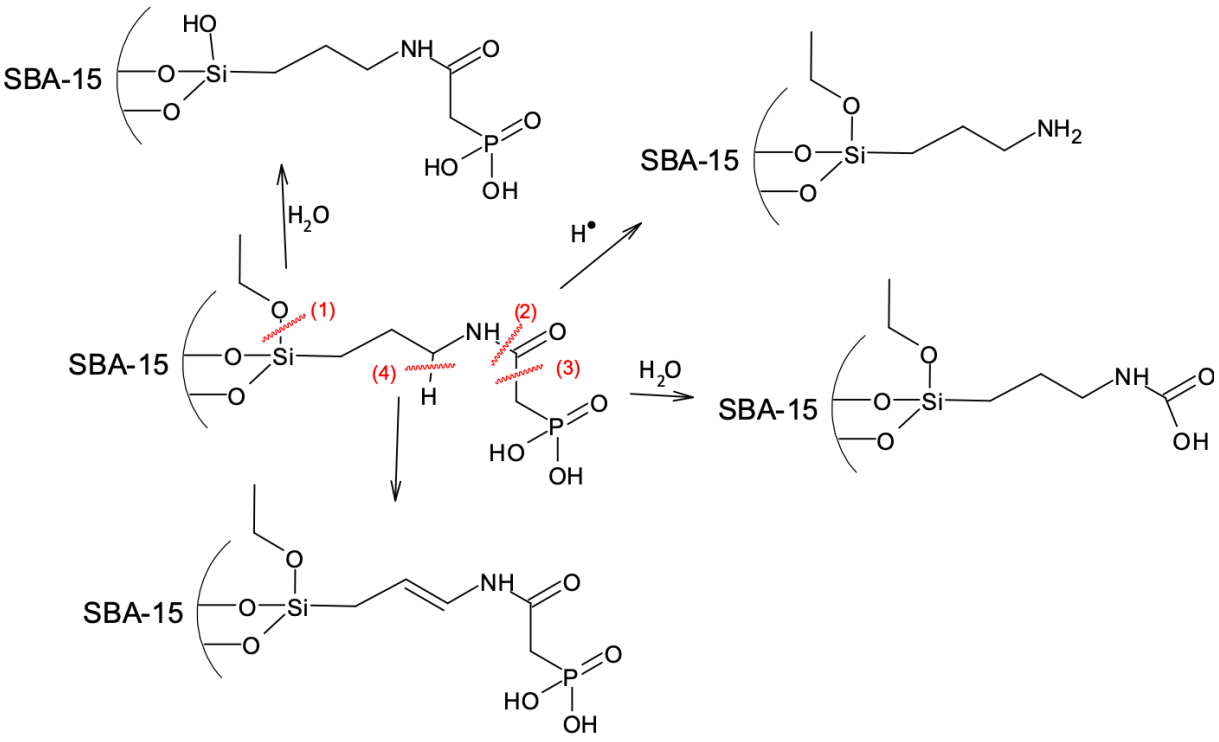

Scheme 2. *Scheme of the main bond cleavages envisioned, illustrated on the SBA-15-Ac-phos sample. (1) Si-O bond cleavage (2) N-C bond cleavage at the amide group (3) C-C bond cleavage between the carbonyl group and the phosphorus atom (4) example of a C-H bond cleavage. Reactions with trace water molecules are described.*

3.2.4. Sorption ability of the irradiated materials

The sorption of thorium was studied in the grafted mesoporous silicas before and after their irradiation and its corresponding sorption ability was assessed. This element was selected to simulate the behavior of plutonium since it has similar chemical behavior (similar (+IV) oxidation state, ionic radius of 108 pm as compared to 100 pm for plutonium) without its high radiotoxicity.

The adsorption isotherms were fitted using both a Langmuir and a Freundlich model, as discussed in the Supplementary Material (Table S5 and Figure S10). The Langmuir model led to better fits to the data, therefore, it was used in the following figures. The model corresponds to a monolayer of sorption of metals at the surface of the adsorbent [60], as frequently encountered during the sorption of metals onto functionalized SBA-15 [14, 60-63].

The adsorption isotherms of thorium are given in Figure 9a for SBA-15-Ac-phos and 9b for SBA-15-Prop-phos, where the equilibrium sorption capacity q_e is plotted as a function of the equilibrium concentration of thorium in the aqueous phase. The pristine SBA-15 materials showed a negligible sorption of thorium as compared to the grafted materials. It was measured to be 7 $mg.g^{-1}$ (or 0.03 $mmol.g^{-1}$). This low sorption ability of pristine mesoporous silica was already reported in the literature [53]. It is due to the large surface area of mesoporous silica and to the formation of Th(IV) complexes with the oxygen atoms of silanol groups. As the SBA-15-HOPO material did not enable any significant extraction of thorium under the present experimental conditions, it was not studied below, despite its good robustness towards ionizing radiation. This indicates that the phosphonate groups are responsible for the thorium adsorption. Obviously, the complexation of Th(IV) with oxygen atoms linked to the phosphorus atom is favorable. Indeed, it occurs thanks to the electrostatic interactions between the deprotonated phosphonate groups [14] and the Th^{4+} and $Th(OH)^{3+}$ species formed in solution within the studied pH range [53].

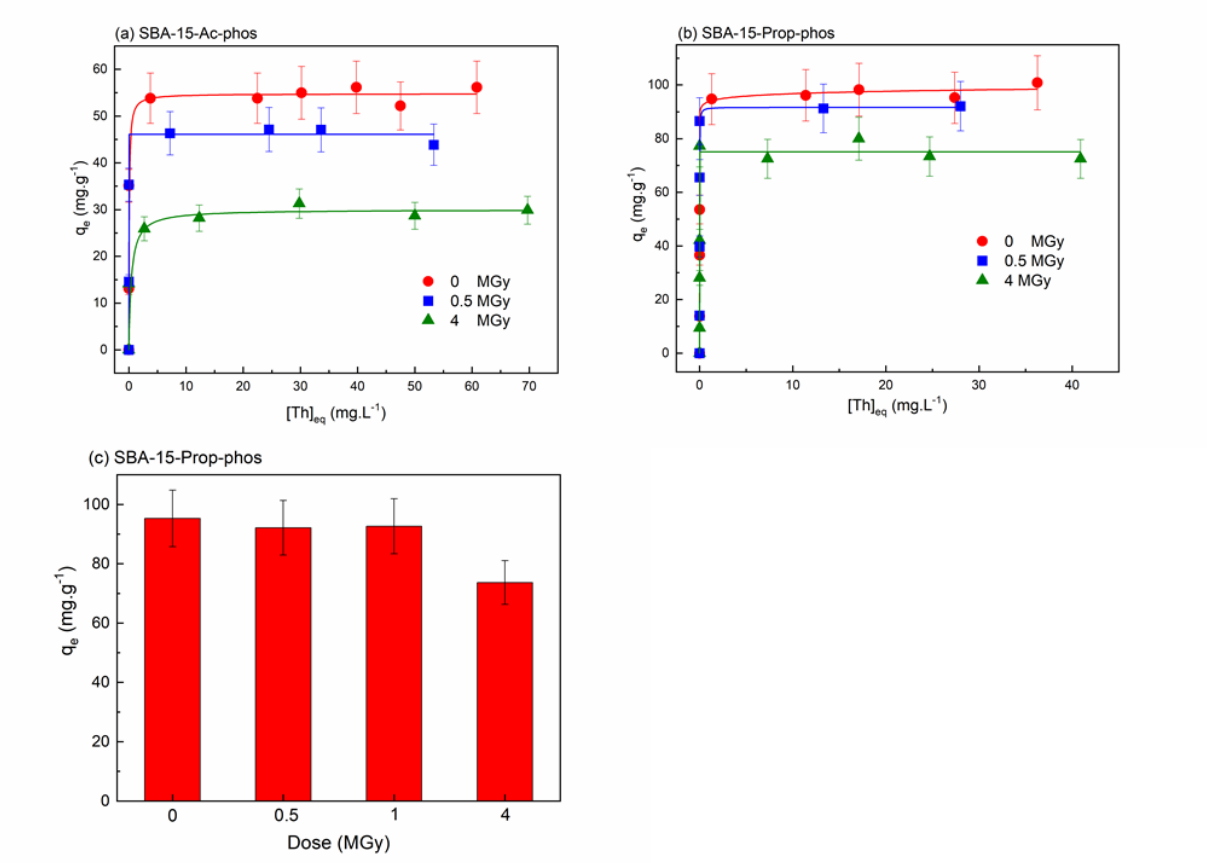

Figure 9. *Adsorption isotherms of Th using SBA-15-Ac-phos (a) or SBA-15-Prop-phos (b) before (0 MGy) and after irradiation at 0.5 MGy and 4 MGy. Data were fitted with a Langmuir model. (c) Adsorption capacity of SBA-15-Prop-phos before (0 MGy) and after irradiation at 0.5 MGy, 1 MGy and 4 MGy with an initial thorium concentration of 80 mg·L^{-1}.*

The curves shown in Figure 9 follow all a similar trend. First, the curves are increasing, indicating that thorium is readily adsorbed into the grafted SBA-15. Secondly, the curves reach a plateau, showing that the maximum sorption ability is reached and that any additional thorium will remain in the aqueous phase. For SBA-15-Ac-phos before irradiation, the maximum q_e value (55 mg·g^{-1}) is reached at an equilibrium concentration of 3.7 mg·L^{-1}. The maximum q_e value (95 mg·g^{-1}) is reached at an equilibrium concentration of 1.3 mg·L^{-1} for SBA-15-Prop-phos before irradiation, corresponding to the incorporation of 9.5 wt% of thorium within the material. SBA-15-Prop-phos shows then the higher adsorption capacity and the highest affinity for thorium (see Table S5 and Figure S10 in Supplementary Material). The equilibrium sorption capacity of Th(IV) towards SBA-15 grafted with Ac-Phos and Prop-phos corresponds to 0.24 and 0.41 mmol.g^{-1}. Knowing the characteristics of the grafted materials (specific area after grafting, grafting density, see Table 1) and neglecting the sorption on silanol groups,

these values correspond in average to 1 Th(IV) for 3.1 ligands and 1 Th(IV) for 1.4 ligand in SBA-15-Ac-phos and SBA-15-Prop-phos, respectively. This result is in accordance with the data from Fryxell *et al.* who found that the adsorption efficiency of Th was twice higher with SBA-15-Prop-phos as compared to SBA-15-Ac-phos [64].

The adsorption efficiency of Th obtained with these material (>90% of Th extracted for Th concentration lower than 50 $mg.L^{-1}$) are comparable to the adsorption efficiency of some ion exchange resins used for the same purpose [65-66].

After irradiation, the sorption behavior of thorium remains unchanged, since all curves have the same shape. However, the sorption ability of SBA-15-Ac-phos is reduced. After irradiation at 500 kGy, the maximum q_e decreases from 55 (before irradiation) to 47 $mg{\cdot}g^{-1}$. It further decreases to 30 $mg{\cdot}g^{-1}$ when the material is irradiated at 4 MGy. Therefore, irradiation and bond cleavage at the amide group (bond ruptures (2) and (3) on Scheme 2) leads to the loss of phosphonate groups, which are interacting with the metal, consequently reducing the sorption ability of the material. The sorption ability of SBA-15-Prop-phos is similar before and after irradiation at 1 MGy, indicating a better resistance towards irradiation than SBA-Ac-phos. We checked that the IR spectra of SBA-15-Prop-phos irradiated at 1 MGy was similar to that of the non-irradiated sample, indicating low damage up to 1 MGy. The sorption ability of SBA-15-Prop-phos was evaluated after irradiation at 0.5 MGy, 1 MGy and 4 MGy, and compared with the sorption ability of the non-irradiated sample (Figure 9(c)). It is similar before and after irradiation up to 1 MGy. However, as evidenced on the adsorption isotherm (Figure 9), sorption is around 20% lower when the material is irradiated up to 4 MGy.

Even if the q_e value of SBA-15-Prop-phos irradiated at 4 MGy is slightly lower (around 75 $mg{\cdot}g^{-1}$) than in the non-irradiated material, indicating that the loss of phosphonate groups has an impact on the sorption ability of the material at this dose, its decrease is significantly smaller than for the SBA-15-Ac-Phos sample (21% decrease for SBA-15-Prop-Phos vs 45% decrease for SBA-15-Ac-Phos after a 4 MGy irradiation). In SBA-15-Prop-phos as compared to SBA-15-Ac-phos, the additional carbon atom linked to the phosphorus one will lead to an increased electron density on this latter atom, therefore improving the interaction with the Th^{4+} and $Th(OH)^{3+}$ species. This can account for the higher sorption ability of SBA-15-Prop-phos as compared to SBA-15-Ac-phos, and also to its more robust behavior under ionizing radiation.

The sorption of metals from industrial wastewaters is usually performed with cation exchange resins. Cation exchange resins bearing salicylic acid groups showed good resistance to radiation, with no change in the sorption behavior of the material up to 2 MGy [67]. Notably, the resistance of ion exchange resins under irradiation strongly depends on their material. Anion exchange resins suffer from severe attrition when the dose reaches 0.1 MGy, while some inorganic ion exchangers such as zeolites retain their retention ability up to a dose of 100 MGy [67]. Most of the organic ion exchangers used for this purpose lose their sorption ability completely when the dose reaches 10 MGy [67]. The results we obtain here are in line with these values. However, grafted mesoporous silicas offer a better selectivity than ion exchange resins as well as a high surface area in a compact volume.

In the context of liquid outflows contaminated by actinides, the sorbent material is submitted to a maximum dose of 100 $Gy \cdot h^{-1}$ [22]. Since the sorption behavior of SBA-15-Prop-phos is relatively unaffected after 1 MGy, this material could be used for at least 10,000 hours (~ 14 months) without any change in its sorption ability. From our results, we can also infer that it could still be used up to a dose of 2 MGy.

4. Conclusion

The degradation and thorium-adsorption behavior of SBA-15 mesoporous silicas grafted with Ac-phos, Prop-phos and 1,2-HOPO ligands was studied under electron irradiation. These ligands were selected based on their ability to bind to actinides, in order to adsorb these radioactive metals from aqueous effluents. Significant differences in the behavior of ligands under irradiation were observed depending on whether they were grafted on the SBA-15 matrix or not. This is due to the fact that exciton transfer from the material to the ligand drives different degradation processes in grafted SBA-15 materials, which lead to selective dissociation channels mainly producing CO. On the contrary, direct radiolysis of the ligand leads preferentially to C-C and C-H bond rupture, mainly producing H_2 and alkanes that were globally less or not detected for grafted SBA-15 samples.

The amide functional group of all three grafted ligands was shown to be preferentially cleft, leading to CO production and to probable fragmentation of the grafted molecule into an

amine. We suggest here also the formation of amic acid under irradiation. Reaction mechanisms induced by ionizing radiation were proposed. From the three grafted mesoporous silicas studied, SBA-15-HOPO was found to be the most resistant towards irradiation, producing the lowest amount of gas, which was attributed to the protective effect of its aromatic ring. However, this sample did not lead to any significant sorption of thorium within the concentration range studied, due to the absence of the phosphonate group. Overall, the sorption capacity of Th(IV) into grafted SBA-15-Prop-phos and SBA-15-Ac-phos was found to decrease when the sample was irradiated. However, the SBA-15-Prop-phos sample evidenced a high sorption of 95 $mg \cdot g^{-1}$ towards thorium. Moreover, its sorption ability remained relatively unchanged for irradiation doses up to at least 1 MGy. The radiation resistance of SBA-15-Prop-phos evidenced in this work is comparable to the most resistant ion exchange resins used for the same purpose. However, grafted mesoporous silicas offer a better selectivity than ion exchange resins as well as a high surface area in a compact volume.

Conflicts of interest

There are no conflicts to declare.

Acknowledgments

Funding from the Agence Nationale de la Recherche (ANR Automact N° ANR-18-CE05-0016-03) is gratefully acknowledged. The authors would like to thank J. Vieira for his help with irradiation experiments, Dr. W. Leibl for FT-IR measurements, Dr. J. Leroy for XPS analysis and F. Carpentier, D. Durand and V. Dauvois for their help with GC-MS. The authors gratefully thank Dr. Mark Levenstein for reading the manuscript and making insightful comments.

References

[1] J. Magill, V. Berthou, D. Haas, J. Galy, R. Schenkel, H.-W. Wiese, G. Heusener, J. Tommasi, G. Youinou, Impact limits of partitioning and transmutation scenarios on the radiotoxicity of actinides in radioactive waste, Nuclear Energy. 42 (2003) 263–277. https://doi.org/10.1680/nuen.42.5.263.37622.

[2] Y. Lin, S.K. Fiskum, W. Yantasee, H. Wu, S.V. Mattigod, E. Vorpagel, G.E. Fryxell, K.N. Raymond, J. Xu, Incorporation of Hydroxypyridinone Ligands into Self-Assembled Monolayers on Mesoporous Supports for Selective Actinide Sequestration, Environ. Sci. Technol. 39 (2005) 1332–1337. https://doi.org/10.1021/es049169t.

[3] R.V. de Pádua Ferreira, S.K. Sakata, F. Dutra, P.B. Di Vitta, M.H.T. Taddei, M.H. Bellini, J.T. Marumo, Treatment of radioactive liquid organic waste using bacteria community, J Radioanal Nucl Chem. 292 (2012) 811–817. https://doi.org/10.1007/s10967-011-1564-2.

[4] S.M. Macgill, The geological disposal of nuclear waste by N. A. Chapman and I. G. McKinley, John wiley & sons, Chichester, 1987, Earth Surf. Process. Landforms. 14 (1989) 755–756. https://doi.org/10.1002/esp.3290140814.

[5] P. Makowski, X. Deschanels, A. Grandjean, D. Meyer, G. Toquer, F. Goettmann, Mesoporous materials in the field of nuclear industry: applications and perspectives, New J. Chem. 36 (2012) 531–541. https://doi.org/10.1039/C1NJ20703B.

[6] V.M. Sawant, V.G. Gaikar, Effective separation of uranyl(II) and thorium(IV) ions from mixtures with neodymium(III) using citric acid and hexabutyl citramide as ligands grafted on mesoporous silica and polystyrene adsorbents, Separation Science and Technology. 55 (2020) 1795–1812. https://doi.org/10.1080/01496395.2019.1614626.

[7] F. Zhang, K.-Q. Ma, Y. Li, Q. Ran, C.-Y. Yao, C.-T. Yang, H.-Z. Yu, S. Hu, S.-M. Peng, Selective separation of thorium from rare earths and uranium in acidic solutions by phosphorodiamidate-functionalized silica, Chemical Engineering Journal. 392 (2020) 123717. https://doi.org/10.1016/j.cej.2019.123717.

[8] J. Florek, S. Giret, E. Juère, D. Larivière, F. Kleitz, Functionalization of mesoporous materials for lanthanide and actinide extraction, Dalton Trans. 45 (2016) 14832–14854. https://doi.org/10.1039/C6DT00474A.

[9] B.E. Johnson, P.H. Santschi, C.-Y. Chuang, S. Otosaka, R.S. Addleman, M. Douglas, R.D. Rutledge, W. Chouyyok, J.D. Davidson, G.E. Fryxell, J.M. Schwantes, Collection of Lanthanides and Actinides from Natural Waters with Conventional and Nanoporous Sorbents, Environ. Sci. Technol. 46 (2012) 11251–11258. https://doi.org/10.1021/es204192r.

[10] J. Veliscek-Carolan, Separation of actinides from spent nuclear fuel: A review, Journal of Hazardous Materials. 318 (2016) 266–281. https://doi.org/10.1016/j.jhazmat.2016.07.027.

[11] G.E. Fryxell, H. Wu, Y. Lin, W.J. Shaw, J.C. Birnbaum, J.C. Linehan, Z. Nie, K. Kemner, S. Kelly, Lanthanide selective sorbents: self-assembled monolayers on mesoporous supports (SAMMS), J. Mater. Chem. 14 (2004) 3356. https://doi.org/10.1039/b408181a.

[12] Q. Gao, J.-F. Xie, Y.-T. Shao, C. Chen, B. Han, K.-S. Xia, C.-G. Zhou, Ultrafast and high-capacity adsorption of Gd(III) onto inorganic phosphorous acid modified mesoporous SBA-15, Chemical Engineering Journal. 313 (2017) 197–206. https://doi.org/10.1016/j.cej.2016.12.068.

[13] Ş. Sert, M. Eral, Uranium adsorption studies on aminopropyl modified mesoporous sorbent (NH2–MCM-41) using statistical design method, Journal of Nuclear Materials. 406 (2010) 285–292. https://doi.org/10.1016/j.jnucmat.2010.08.024.

[14] Y.-L. Wang, L. Zhu, B.-L. Guo, S.-W. Chen, W.-S. Wu, Mesoporous silica SBA-15 functionalized with phosphonate derivatives for uranium uptake, New J. Chem. 38 (2014) 3853–3861. https://doi.org/10.1039/C3NJ01494K.

[15] G. Xue, F. Yurun, M. Li, G. Dezhi, J. Jie, Y. Jincheng, S. Haibin, G. Hongyu, Z. Yujun, Phosphoryl functionalized mesoporous silica for uranium adsorption, Applied Surface Science. 402 (2017) 53–60. https://doi.org/10.1016/j.apsusc.2017.01.050.

[16] W. Yantasee, G.E. Fryxell, K. Pattamakomsan, T. Sangvanich, R.J. Wiacek, B. Busche, R.S. Addleman, C. Timchalk, W. Ngamcherdtrakul, N. Siriwon, Selective capture of radionuclides (U, Pu, Th, Am and Co) using functional nanoporous sorbents, Journal of Hazardous Materials. 366 (2019) 677–683. https://doi.org/10.1016/j.jhazmat.2018.12.043.

[17] J. Aguado, J.M. Arsuaga, A. Arencibia, M. Lindo, V. Gascón, Aqueous heavy metals removal by adsorption on amine-functionalized mesoporous silica, Journal of Hazardous Materials. 163 (2009) 213–221. https://doi.org/10.1016/j.jhazmat.2008.06.080.

[18] Y. Lou, G. Toquer, S. Dourdain, C. Rey, C. Grygiel, D. Simeone, X. Deschanels, Structure evolution of mesoporous silica SBA-15 and MCM-41 under swift heavy ion irradiation, Nuclear Instruments and Methods in Physics Research Section B: Beam Interactions with Materials and Atoms. 365 (2015) 336–341. https://doi.org/10.1016/j.nimb.2015.08.009.

[19] J. Lin, G. Toquer, C. Grygiel, S. Dourdain, Y. Guari, C. Rey, J. Causse, X. Deschanels, Behavior of mesoporous silica under 2 MeV electron beam irradiation, Microporous and Mesoporous Materials. 328 (2021) 111454. https://doi.org/10.1016/j.micromeso.2021.111454.

[20] J.C. Birnbaum, B. Busche, Y. Lin, W.J. Shaw, G.E. Fryxell, Synthesis of carbamoylphosphonate silanes for the selective sequestration of actinides, Chem. Commun. (2002) 1374–1375. https://doi.org/10.1039/b200186c.

[21] C. Shi, X. Wang, J. Wan, D. Zhang, X. Yi, Z. Bai, K. Yang, J. Diwu, Z. Chai, S. Wang, 3,2-Hydroxypyridinone-Grafted Chitosan Oligosaccharide Nanoparticles as Efficient Decorporation Agents for Simultaneous Removal of Uranium and Radiation-Induced Reactive Oxygen Species *in Vivo*, Bioconjugate Chem. 29 (2018) 3896–3905. https://doi.org/10.1021/acs.bioconjchem.8b00711.

[22] J. Sejvar, Normal Operating Radiation Levels in Pressurized Water Reactor Plants, Nuclear Technology. 36 (1977) 48–55. https://doi.org/10.13182/NT77-A31957.

[23] S. Iqbal, J.-I. Yun, Decontamination of radionuclides by functionalized mesoporous silica under gamma irradiation, RSC Adv. 8 (2018) 32211–32220. https://doi.org/10.1039/C8RA05939J.

[24] M. Bruce, M. Davis, Radiation effects on organic materials in nuclear plants. Final report, 1981. https://doi.org/10.2172/5591289.

[25] W.J. Weber, Radiation and Thermal Ageing of Nuclear Waste Glass, Procedia Materials Science. 7 (2014) 237–246. https://doi.org/10.1016/j.mspro.2014.10.031.

[26] W.J. Weber, Radiation effects in nuclear waste glasses, Nuclear Instruments and Methods in Physics Research Section B: Beam Interactions with Materials and Atoms. 32 (1988) 471–479. https://doi.org/10.1016/0168-583X(88)90257-1.

[27] S. Iqbal, J.-I. Yun, EDTA-functionalized mesoporous silica for the removal of corrosion products: Adsorption studies and performance evaluation under gamma irradiation, Microporous and Mesoporous Materials. 248 (2017) 149–157. https://doi.org/10.1016/j.micromeso.2017.04.028.

[28] W. Zhang, G. Ye, J. Chen, Study on the gamma-ray irradiation behavior of mesoporous silica adsorbents functionalized with phosphine oxide and phosphonic acid ligands, J Radioanal Nucl Chem. 307 (2016) 1445–1451. https://doi.org/10.1007/s10967-015-4249-4.

[29] S. Le Caër, F. Brunet, C. Chatelain, D. Durand, V. Dauvois, T. Charpentier, J. Ph. Renault, Modifications under Irradiation of a Self-Assembled Monolayer Grafted on a Nanoporous Silica Glass: A Solid-State NMR Characterization, J. Phys. Chem. C. 116 (2012) 4748–4759. https://doi.org/10.1021/jp211639u.

[30] S. Le Caër, F. Brunet, C. Chatelain, L. Ladevie, D. Durand, V. Dauvois, J.Ph. Renault, T. Charpentier, Influence of the Nature of Self-Assembled Monolayers on Their Reactivity under Ionizing Radiation: A Solid-State NMR Study, J. Phys. Chem. C. 117 (2013) 23258–23271. https://doi.org/10.1021/jp4056335.

[31] N. Brodie-Linder, S. Le Caër, M.S. Alam, J.P. Renault, C. Alba-Simionesco, H2 formation by electron irradiation of SBA-15 materials and the effect of CuII grafting, Phys. Chem. Chem. Phys. 12 (2010) 14188. https://doi.org/10.1039/c0cp00115e.

[32] D. Zhao, J. Feng, Q. Huo, N. Melosh, G.H. Fredrickson, B.F. Chmelka, G.D. Stucky, Triblock Copolymer Syntheses of Mesoporous Silica with Periodic 50 to 300 Angstrom Pores, Science. 279 (1998) 548–552. https://doi.org/10.1126/science.279.5350.548.

[33] J.S. Beck, J.C. Vartuli, W.J. Roth, M.E. Leonowicz, C.T. Kresge, K.D. Schmitt, C.T.W. Chu, D.H. Olson, E.W. Sheppard, S.B. McCullen, J.B. Higgins, J.L. Schlenker, A new family of mesoporous molecular sieves prepared with liquid crystal templates, J. Am. Chem. Soc. 114 (1992) 10834–10843. https://doi.org/10.1021/ja00053a020.

[34] M.J. Cook, A.R. Katritzky, P. Linda, R.D. Tack, Aromaticity and tautomerism. Part I. The aromatic resonance energy of 2-pyridone and the related thione, methide, and imine, J. Chem. Soc., Perkin Trans. 2. (1972) 1295. https://doi.org/10.1039/p29720001295.

[35] Handbook of Nuclear Chemistry: Basics of Nuclear Science ; Elements and Isotopes: Formation, Transformation, Distribution ; Chemical Applications of Nuclear Reactions and Radiations ; Radiochemistry and Radiopharmaceutical Chemistry in Life Sciences ; Instrumentation, Separation Techniques, Environmental Issues., 2004. https://doi.org/10.1007/0-387-30682-X (accessed December 9, 2021).

[36] Y. Sánchez-Vicente, L. Stevens, C. Pando, A. Cabañas, Functionalization of Silica SBA-15 with [3-(2-Aminoethylamino)Propyl] Trimethoxysilane in Supercritical CO2 Modified with Methanol or Ethanol for Carbon Capture, Energies. 13 (2020) 5804. https://doi.org/10.3390/en13215804.

[37] U.D. Thach, P. Hesemann, G. Yang, A. Geneste, S. Le Caër, B. Prelot, Ionosilicas as efficient sorbents for anionic contaminants: Radiolytic stability and ion capacity, Journal of Colloid and Interface Science. 482 (2016) 233–239. https://doi.org/10.1016/j.jcis.2016.07.069.

[38] J.W.T. Spinks, R.J. Woods, An introduction to radiation chemistry, 3rd ed, Wiley, New York, 1990.

[39] S. Le Caër, G. Vigneron, D. Guillaumont, L. Berthon, N. Zorz, P. Moisy, Experimental and theoretical study of the degradation of malonamide extractant molecules under ionizing radiation, RSC Adv. 2 (2012) 3954. https://doi.org/10.1039/c2ra01201d.

[40] S.B. Dhiman, J.A. LaVerne, Radiolysis of simple quaternary ammonium salt components of Amberlite resin, Journal of Nuclear Materials. 436 (2013) 8–13. https://doi.org/10.1016/j.jnucmat.2013.01.294.

[41] A.B. Patil, P. Pathak, V.S. Shinde, S.V. Godbole, P.K. Mohapatra, Efficient solvent system containing malonamides in room temperature ionic liquids: actinide extraction, fluorescence and radiolytic degradation studies, Dalton Trans. 42 (2013) 1519–1529. https://doi.org/10.1039/C2DT32186F.

[42] I.A. Shkrob, T.W. Marin, Electron Localization and Radiation Chemistry of Amides, J. Phys. Chem. A. 116 (2012) 1746–1757. https://doi.org/10.1021/jp2115687.

[43] I.A. Shkrob, T.W. Marin, J.R. Bell, H. Luo, S. Dai, J.L. Hatcher, R.D. Rimmer, J.F. Wishart, Radiation-Induced Fragmentation of Diamide Extraction Agents in Ionic Liquid Diluents, J. Phys. Chem. B. 116 (2012) 2234–2243. https://doi.org/10.1021/jp2117483.

[44] J.A. Drader, N. Boubals, B. Camès, D. Guillaumont, P. Guilbaud, G. Saint-Louis, L. Berthon, Radiolytic stability of *N* , *N* -dialkyl amide: effect on Pu(IV) complexes in solution, Dalton Trans. 47 (2018) 251–263. https://doi.org/10.1039/C7DT03447D.

[45] G.P. Horne, S.P. Mezyk, B.J. Mincher, C.A. Zarzana, C. Rae, R.D. Tillotson, N.C. Schmitt, R.D. Ball, J. Ceder, M.-C. Charbonnel, P. Guilbaud, G. Saint-Louis, L. Berthon, DEHBA (di-2-ethylhexylbutyramide) gamma radiolysis under spent nuclear fuel solvent extraction process conditions, Radiation Physics and Chemistry. 170 (2020) 108608. https://doi.org/10.1016/j.radphyschem.2019.108608.

[46] R. Chiarizla, E.P. Horwltz, hydrolytic and radiolytic degradation of octyl(phenyl)-N,N-diiso-butylcarbamoylmethylphosphine oxide and related compounds, Solvent Extraction and Ion Exchange. 4 (1986) 677–723. https://doi.org/10.1080/07366298608917888.

[47] B.J. Mincher, G. Modolo, S.P. Mezyk, Review Article: The Effects of Radiation Chemistry on Solvent Extraction 3: A Review of Actinide and Lanthanide Extraction, Solvent Extraction and Ion Exchange. 27 (2009) 579–606. https://doi.org/10.1080/07366290903114098.

[48] A.S. Maria Chong, X.S. Zhao, Functionalization of SBA-15 with APTES and Characterization of Functionalized Materials, J. Phys. Chem. B. 107 (2003) 12650–12657. https://doi.org/10.1021/jp035877+.

[49] N.B. Colthup, L.H. Daly, S.E. Wiberley, Introduction to Infrared and Raman Spectroscopy., Elsevier Science, Burlington, 1990. https://public.ebookcentral.proquest.com/choice/publicfullrecord.aspx?p=1179808 (accessed October 30, 2021).

[50] S. Qi, Z. Wu, D. Wu, W. Yang, R. Jin, The chemistry involved in the loading of silver(I) into poly(amic acid) via ion exchange: A metal-ion-induced crosslinking behavior, Polymer. 50 (2009) 845–854. https://doi.org/10.1016/j.polymer.2008.12.010.

[51] Y.-C. Kung, S.-H. Hsiao, Solution-processable, high-T $_g$, ambipolar polyimide electrochromics bearing pyrenylamine units, J. Mater. Chem. 21 (2011) 1746–1754. https://doi.org/10.1039/C0JM02642E.

[52] M.J. Ariza, E. Rodríguez-Castellón, R. Rico, J. Benavente, M. Muñoz, M. Oleinikova, X-Ray Photoelectron Spectroscopy Analysis of Di-(2-ethylhexyl) Phosphoric Acid Activated Membranes, Journal of Colloid and Interface Science. 226 (2000) 151–158. https://doi.org/10.1006/jcis.2000.6805.

[53] L.-Y. Yuan, Z.-Q. Bai, R. Zhao, Y.-L. Liu, Z.-J. Li, S.-Q. Chu, L.-R. Zheng, J. Zhang, Y.-L. Zhao, Z.-F. Chai, W.-Q. Shi, Introduction of Bifunctional Groups into Mesoporous Silica for Enhancing Uptake of Thorium(IV) from Aqueous Solution, ACS Appl. Mater. Interfaces. 6 (2014) 4786–4796. https://doi.org/10.1021/am405584h.

[54] S.K. Das, C. Dickinson, F. Lafir, D.F. Brougham, E. Marsili, Synthesis, characterization and catalytic activity of gold nanoparticles biosynthesized with Rhizopus oryzae protein extract, Green Chem. 14 (2012) 1322. https://doi.org/10.1039/c2gc16676c.

[55] R.H. Partridge, Excitation Energy Transfer in Alkanes. III. Radiation Chemistry of Alkane Polymers, The Journal of Chemical Physics. 52 (1970) 2501–2510. https://doi.org/10.1063/1.1673334.

[56] M. Alam, F. Miserque, M. Taguchi, L. Boulanger, J.P. Renault, Tuning hydrogen production during oxide irradiation through surface grafting, J. Mater. Chem. 19 (2009) 4261. https://doi.org/10.1039/b901936g.

[57] Z.A. Weinberg, G.W. Rubloff, E. Bassous, Transmission, photoconductivity, and the experimental band gap of thermally grown Si O 2 films, Phys. Rev. B. 19 (1979) 3107–3117. https://doi.org/10.1103/PhysRevB.19.3107.

[58] N.A. Lange, Lange's handbook of chemistry, 15. ed, McGraw-Hill, New York, NY, 1999.

[59] C.S. Dulcey, J.H. Georger, V. Krauthamer, D.A. Stenger, T.L. Fare, J.M. Calvert, Deep UV Photochemistry of Chemisorbed Monolayers: Patterned Coplanar Molecular Assemblies, Science. 252 (1991) 551–554. https://doi.org/10.1126/science.2020853.

[60] A. Shahbazi, H. Younesi, A. Badiei, Functionalized SBA-15 mesoporous silica by melamine-based dendrimer amines for adsorptive characteristics of Pb(II), Cu(II) and Cd(II) heavy metal ions in batch and fixed bed column, Chemical Engineering Journal. 168 (2011) 505–518. https://doi.org/10.1016/j.cej.2010.11.053.

[61] O. Dudarko, N. Kobylinska, B. Mishra, V.G. Kessler, B.P. Tripathi, G.A. Seisenbaeva, Facile strategies for synthesis of functionalized mesoporous silicas for the removal of rare-earth elements and heavy metals from aqueous systems, Microporous and Mesoporous Materials. 315 (2021) 110919. https://doi.org/10.1016/j.micromeso.2021.110919.

[62] H. Wu, Y. Xiao, Y. Guo, S. Miao, Q. Chen, Z. Chen, Functionalization of SBA-15 mesoporous materials with 2-acetylthiophene for adsorption of Cr(III) ions, Microporous and Mesoporous Materials. 292 (2020) 109754. https://doi.org/10.1016/j.micromeso.2019.109754.

[63] M.A. Betiha, Y.M. Moustafa, M.F. El-Shahat, E. Rafik, Polyvinylpyrrolidone-Aminopropyl-SBA-15 schiff Base hybrid for efficient removal of divalent heavy metal cations from

wastewater, Journal of Hazardous Materials. 397 (2020) 122675. https://doi.org/10.1016/j.jhazmat.2020.122675.

[64] G.E. Fryxell, Y. Lin, S. Fiskum, J.C. Birnbaum, H. Wu, K. Kemner, S. Kelly, Actinide Sequestration Using Self-Assembled Monolayers on Mesoporous Supports, Environ. Sci. Technol. 39 (2005) 1324–1331. https://doi.org/10.1021/es049201j.

[65] K.L. Ang, D. Li, A.N. Nikoloski, The effectiveness of ion exchange resins in separating uranium and thorium from rare earth elements in acidic aqueous sulfate media. Part 1. Anionic and cationic resins, Hydrometallurgy. 174 (2017) 147–155. https://doi.org/10.1016/j.hydromet.2017.10.011.

[66] K.L. Ang, D. Li, A.N. Nikoloski, The effectiveness of ion exchange resins in separating uranium and thorium from rare earth elements in acidic aqueous sulfate media. Part 2. Chelating resins, Minerals Engineering. 123 (2018) 8–15. https://doi.org/10.1016/j.mineng.2018.04.017.

[67] K.K.S. Pillay, A review of the radiation stability of ion exchange materials, Journal of Radioanalytical and Nuclear Chemistry, Articles. 102 (1986) 247–268. https://doi.org/10.1007/BF02037966.